AWARD NUMBER: W81XWH-16-1-0143

TITLE: Auditory Cortical Network Changes in Tinnitus

PRINCIPAL INVESTIGATOR: Patrick O. Kanold

CONTRACTING ORGANIZATION: University of Maryland, College Park
College Park, MD 20742

REPORT DATE: June 2018

TYPE OF REPORT: Final

PREPARED FOR: U.S. Army Medical Research and Materiel Command
Fort Detrick, Maryland 21702-5012

REPORT DOCUMENTATION PAGE

Form Approved
OMB No. 0704-0188

1. REPORT DATE	2. REPORT TYPE	3. DATES COVERED
June 2018	Final	1 Sep 2016 – 28 Feb 2018

4. TITLE AND SUBTITLE

Auditory Cortical Network Changes in Tinnitus

5a. CONTRACT NUMBER
W81XWH-16-1-0143

5b. GRANT NUMBER

5c. PROGRAM ELEMENT NUMBER

6. AUTHOR(S)
Patrick O. Kanold

E-Mail:pkanold@umd.edu

5d. PROJECT NUMBER

5e. TASK NUMBER

5f. WORK UNIT NUMBER

7. PERFORMING ORGANIZATION NAME(S) AND ADDRESS(ES)

UNIVERSITY OF MARYLAND
3112 LEE BLDG 7809 REGENTS DR
COLLEGE PARK MD 20742-0001

8. PERFORMING ORGANIZATION REPORT NUMBER

9. SPONSORING / MONITORING AGENCY NAME(S) AND ADDRESS(ES)

U.S. Army Medical Research and Materiel Command
Fort Detrick, Maryland 21702-5012

10. SPONSOR/MONITOR'S ACRONYM(S)

11. SPONSOR/MONITOR'S REPORT NUMBER(S)

12. DISTRIBUTION / AVAILABILITY STATEMENT

Approved for Public Release; Distribution Limited

13. SUPPLEMENTARY NOTES

14. ABSTRACT

We proposed to study the impact of noise trauma on neuronal circuits in the auditory cortex of mice. During the award period, we have demonstrated progress in the following areas as related to the Statement of Work. First, we have used 2-photon laser scanning microscopy (2PLSM) techniques to measure population activity of cortical Layer 2/3 neurons in control animals. We found that neuronal populations in L2/3 display a sparse representation of sound frequency in which neurons are selective, sparse, and perhaps carry increasingly higher amounts of stimulus information as activity moves through cortical layers. Second, we have enhanced our capabilities for behavioral testing by building hardware and software for two additional testing stations. Third, using 2PLSM techniques we have measured neuronal activity in specific subpopulations of inhibitory neurons in L2/3 (i.e., those expressing parvalbumin, PV, somatostatin, SOM, vasoactive intestinal peptide, VIP). We have characterized gap detection behavior of multiple cohorts of mice and obtained stable baseline data in all of them. Our noise overexposure protocol has not produced animals that display behavioral evidence of chronic tinnitus. Future work will aim at using operant conditioning paradigms to test for behavioral evidence of chronic tinnitus.

15. SUBJECT TERMS

None Listed

16. SECURITY CLASSIFICATION OF:			17. LIMITATION OF ABSTRACT	18. NUMBER OF PAGES	19a. NAME OF RESPONSIBLE PERSON
a. REPORT	b. ABSTRACT	c. THIS PAGE			USAMRMC
Unclassified	Unclassified	Unclassified	Unclassified	51	19b. TELEPHONE NUMBER *(include area code)*

TABLE OF CONTENTS

1. **INTRODUCTION:**

Tinnitus is frequently seen after noise trauma to the ear. A core hypothesis of the etiology of tinnitus is that 'ringing in the ears' is generated by increased spontaneous activity and reorganization of normal brain circuits such that the activity of the brain is altered. Current support for this hypothesis exists only at the level of individually recorded single neurons, which show increased spontaneous neural activity and changes in sensory driven neural responses after noise trauma. Ultimately, however, our perception (including phantom perceptions, like tinnitus) is the result of the collective activity of large numbers of neurons, raising the essential question of how the percept of tinnitus arises from the altered network activity and interactions of populations of neurons. To study neuronal interactions within populations, we proposed to measure activity across many neurons simultaneously. We use two-photon laser scanning microscopy (2PLSM) to simultaneously monitor auditory cortical networks consisting of hundreds of neurons in mice with and without tinnitus-like behavior and identify which circuits are malfunctioning within primary auditory cortex (A1). To achieve this we will go beyond analyzing the responses of single neurons and use population analysis methods including pairwise interactions (e.g. correlations) and cutting edge scale-invariant approaches (e.g. neuronal avalanches) to fill a void in our understanding of the precise changes auditory cortical networks undergo after noise trauma.

2. **KEYWORDS:**

2PLSM – 2-photon laser scanning microscopy
L2/3 – Layer 2/3 of cortex
A1 – primary auditory cortex
GECI – Genetically Encoded Calcium Indicator
GCaMP6 – most advanced/sensitive GECI available
Gap detection – gap pre-pulse inhibition of acoustic startle

3. **ACCOMPLISHMENTS:**

- **What were the major goals of the project?**

The major goals of the project were to use advance optical imaging approaches (2-photon laser scanning microscopy) to:

1) Measure activity of layer 2/3 (L2/3) pyramidal neurons in control mice and mice with behavioral evidence of tinnitus due to noise over-exposure.
2) Measure activity of genetically targeted inhibitory neurons in L2/3 in control mice and mice with behavioral evidence of tinnitus due to noise over-exposure.
3) Measure inhibitory receptive fields of pyramidal neurons in L2/3 in control mice and mice with behavioral evidence of tinnitus due to noise over-exposure.

a. **What was accomplished under these goals?**

We performed 2PLSM imaging experiments in control mice while addressing challenges associated with generating mice Our objective was to identify and establish features of cortical network activity among populations of excitatory and inhibitory L2/3 neurons in the primary auditory cortex (A1) that could serve as a benchmark for comparison against mice with behavioral evidence of tinnitus. To accomplish this we measured ongoing and sound evoked activity in populations of pyramidal neurons as well genetically identified inhibitory neurons (VIP) in A1 in awake, control mice using a genetically encoded calcium indicator (or GECI, i.e., GCaMP6s). To control for the effects of either transgenic expression or viral transfection we compared two cohorts of mice in which the GECI was expressed either via viral injection, or through transgenic methods (Fig 1a-d). While we initially proposed to only investigate L2/3 we found that our transgenic animals also had good expression in L4. We thus also imaged L4.

We found that ongoing activity in L2/3 AND L4 neuronal populations in A1 of control mice display activity patterns whose size and duration are scale-invariant, a signature of critical system balanced between order and disorder (Figs. 1-3). We also find that inhibitory VIP neurons in A1 show sound evoked responses (Fig. 4). This finding in control animals provides a basis for comparison with animals displaying behavioral evidence of tinnitus. Moreover, we did not find large differences between transgenic or viral expression of GECIs. These results set an important baseline for many studies of auditory processing. We have submitted a manuscript based on these findings (see attached).

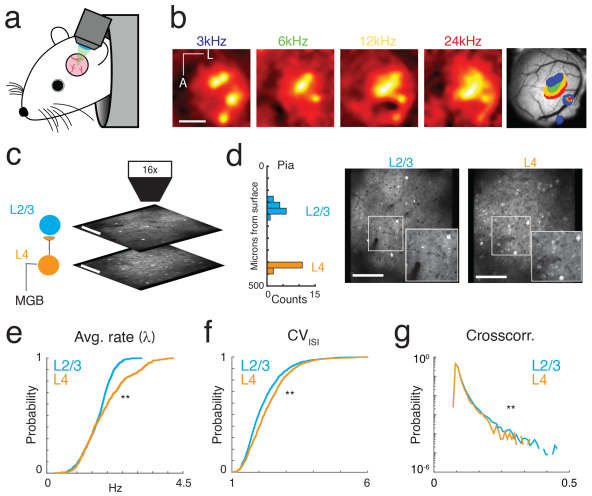

Figure 1. Imaging A1 population activity in the awake mouse. a, Cartoon of awake mouse under the microscope. **b,** Wide-field functional imaging identifies A1. Average activation maps from 4 different sound frequencies and thresholded activity overlaid on image of brain surface. Tonotopic gradient indicates location of A1. Scale bar=1mm. **c,** Imaging L4 and L2/3. Histogram shows distribution of imaging plane depths across all experiments. **d,** Representative fields of view from L2/3 (left) and L4 (right) showing GCaMP6s expression present in both layers. Scale bar: 100μm. **e,** Cumulative probability distributions of average λ for all recorded neurons in L2/3 (blue) and L4 (orange). **f,** Cumulative probability distribution of inferred CV inter-spike interval (CV_{ISI}) for all neurons in L4 (orange) and L2/3 (blue). **g,** Probability distribution of pairwise cross-correlation values for all neurons and experiments for L4 (orange) and L2/3 (blue).

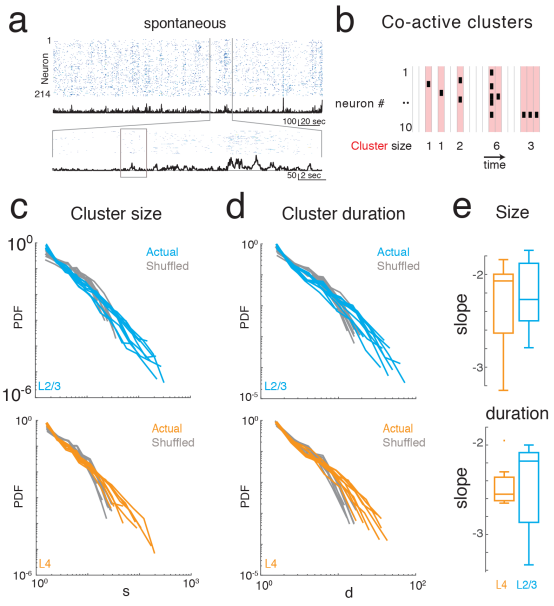

Figure 2. Imaging neuronal ensemble activity in awake mouse A1. a, *Top:* Spike density raster plot of ongoing activity recorded from L2/3 pyramidal neurons with corresponding population activities (black). *Middle:* Expanded view of raster plot revealing variable ongoing activity with population activities. **b,** Schematic depicting definition of activity clusters from neuronal activity rasters. Activity from successive time bins/frame in which at least one neuron is firing is concatenated into an activity cluster. Clusters are separated by at least 1 frame with no activity. Vertical gray lines indicate boundaries of frame acquisition (Δt, 33 ms). Shading indicates occurrence of clusters of activity in the network. Cluster sizes indicated below. **c,** Probability distributions of cluster sizes from individual experiments in L4 and in L2/3. Gray lines indicate distributions from shuffled data. **d**, Probability distributions of activity cluster duration of ongoing activity from individual experiments in L2/3 and in L4. Gray lines indicate distributions from shuffled data. **e,** Boxplots showing slopes (α) of probability distributions in cluster size (*top*) and branching parameter (σ; *bottom*) for each experiment in , $\alpha_{L2/3}$: –2.04 ± 0.088, α_{L4}: –2.03 ± 0.11, p>0.5, unpaired two-sample t-test; mean ± std; σ_{L4} = 0.75 ± 0.13, $\sigma_{L2/3}$ = 0.66 ± 0.04. *L4*: magenta; *L2/3*: black. *Circles*: individual experiments.

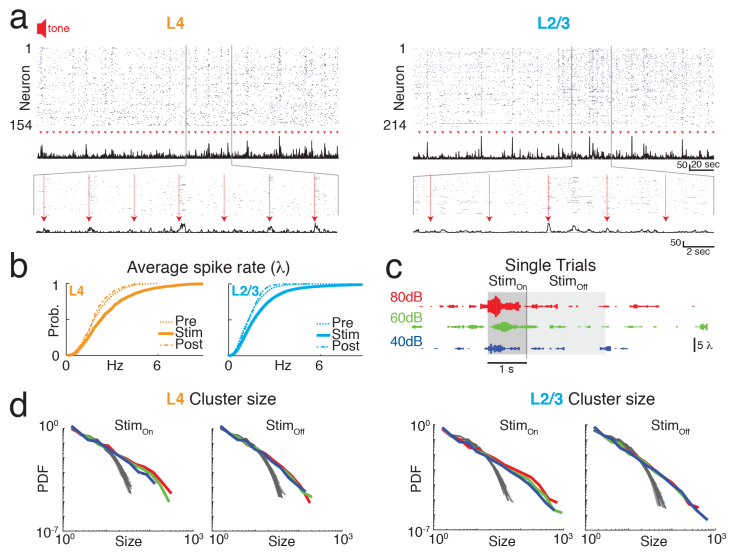

Figure 3. Neuronal ensembles in A1 during ongoing activity organize as neuronal avalanches. **a,** Spike density raster of simultaneously recorded L4 (*left*) and L2/3 (*right*) neurons to brief auditory inputs (*arrow heads*). *Middle*: Corresponding population activities summed over all neurons. *Bottom*: Enlarged views revealing variable, transient evoked responses. **b,** Stimulation (*Stim*) induces transient rate increases in L4 and L2/3 with post-stimulus rates (*post*) returning to pre-stim baseline (*pre*). Cumulative spike probability plots (all neurons). **c,** Examples of intermittent spiking during stim off at all three sound levels. Single trial time course of the number of active neurons per frame (L2/3) at three different sound levels. **d,** Probability density distributions of spike cluster sizes reveal power laws for $Stim_{On}$ and $Stim_{Off}$ conditions and different sound intensity in L4 (*left*) and L2/3 (*right*). Gray lines indicate probability density distributions from shuffled data sets.

Because VIP neurons control a disinhibitory circuit in A1 they are putative targets of tinnitus. We thus aimed to image VIP neurons. We succeeded in imaging inhibitory VIP neurons in control animals (Fig 4).

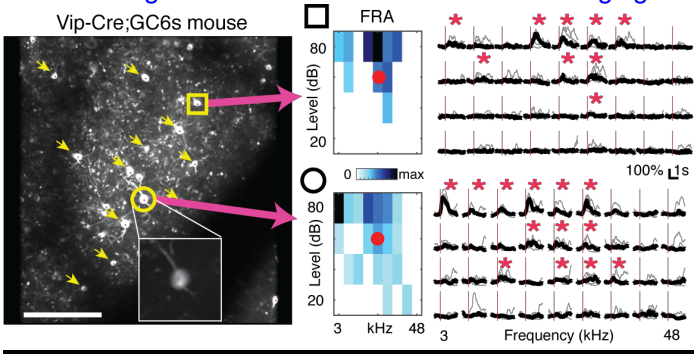

Figure 4. Measurement of VIP+ interneuron sound evoked activity. Left: Average image of imaging plane. Scale: 100μm. Arrowheads: GCaMP6 expressing VIP+ neurons. Right: Frequency response areas and evoked responses for 2 VIP+ interneurons (indicated by circle and square). Red dots: preferred frequency. Red Asterisks: significant response. Gray lines: single trials, black lines: average. Red lines: sound onset.

We implemented a behavioral paradigm (gap detection) to test auditory behavior in mice. This gap detection paradigm is widely used by others to identify behavioral manifestations of tinnitus. We tested animals over many months (sometimes multiple times per week) and in some animals of our tested cohorts of control animals achieved stable baseline.

We implemented our noise over-exposure protocol in multiple cohorts of mice. On all mice we collected extensive baseline data over many weeks to exclude effects of normal variability.

Our sound exposure sessions *failed to produce sufficient subjects* with significant behavioral evidence of chronic tinnitus – the expected yield is ~50% to perform imaging. In one cohort we obtained 3/7 mice with evidence of tinnitus, but other cohorts did not show changes. To perform 2P imaging we need to implant cranial windows which then need to remain clear for many weeks. The success of this procedure is ~30%. Thus 3 mice were not sufficient to image.

As detailed in our progress report from Oct 2017 due the presence of large amounts of behavioral variability we consulted with experts in the field (see below). At their suggestion we spent significant time restructuring our behavioral testing paradigm, changing hardware, and changing our analysis software. Despite these efforts we still failed to detect robust behavioral evidence of tinnitus in subsequent cohorts.

Thus, despite our efforts to achieve stable tinnitus like behavior on noise exposed mice, we failed to do so.

Based on our experience in control mice (Fig. 1-3) we estimate that we need to image 10-15 animals to acquire sufficient data. This means we need to implant ~40 animals with behavioral evidence of tinnitus. Since we did not have sufficient mice showing behavioral evidence of tinnitus, we could not

implant them and image them. Thus, we did not meet our goal of imaging in mice showing behavioral evidence of tinnitus.

We conclude that gap detection paradigms might not be sensitive enough with our exposure paradigm and our mice to detect behavioral effects and thus produce sufficient mice for our purpose. Indeed, recently (after conclusion of this grant) a manuscript was published detailing potential sources of variability such as circadian or estrus cycle, facilitation in subsets of animals, etc. (Longenecker et al.; Hearing Res, 2018 Jun;363:119-135). However, even these studies only addressed variability over 3 weeks. We feel that for a stable percept like tinnitus behavioral changes should last beyond 3 weeks.

Moreover, we also need longer time windows (>4 weeks) due to our cranial window surgery which potentially introduces even more variability. Moreover, we use transgenics for imaging which are on a mixed background (Bl6/CBA). This might introduce additional variability.

Moreover, additional recent studies show that even non-exposed animals can show "tinnitus" behavior while noise exposed animals did not show changes(see Jones A, May BJ; "Effects of Acoustic Environment on Tinnitus Behavior in Sound-Exposed Rats" J Assoc. Res. Otolaryngology. 2018 Apr;19(2):133-146"). These observations match ours and together suggest that other behavioral assays might be needed.

Thus, the future, we aim to use operant conditioning tasks that have been recently suggested to be better to screen for tinnitus (Jones A, May BJ. "Improving the Reliability of Tinnitus Screening in Laboratory Animals"; J Assoc. Res. Otolaryngology. 2017 Feb;18(1):183-195; Lauer AM, Larkin G, Jones A, May BJ; "Behavioral Animal Model of the Emotional Response to Tinnitus and Hearing Loss", J Assoc. Res. Otolaryngology. 2018 Feb;19(1):67-81). As part of our other projects we have recently implemented operant conditioning in the lab which allow us careful psychophysical assessment of auditory function across the hearing range of the mouse (see Francis et al. 2018). We thus hope that in the future we can use this as a more sensitive screen for tinnitus. Moreover, a large number of animals needs to be behaviorally evaluated (~100, see above) which turns out to be more labor intensive than expected. Thus, we believe that automated behavioral testing will be required to longitudinally test large numbers of control and noise exposed animals. We obtained an NIH R21 to allow us to build and test such systems.

Dr. Winkowski applied for NIH R21 funding to continue this tinnitus project, but unfortunately, this application was unsuccessful.

b. **What opportunities for training and professional development has the project provided?**
Training activities:
Mr. James Narin (full time technician) was hired to perform behavioral testing of mice for the project. He received training directly from Dr. Daniel Winkowski (co-PI) on the design, development, and implementation of hardware and software for conducting behavioral testing. After receiving this training, Mr. Narin designed and built two additional testing stations in order to increase throughput for the project.
Dr. Winkowski learned the behavioral assessment of mice and population analysis.

c. **How were the results disseminated to communities of interest?**
Nothing to report
d. **What do you plan to do during the next reporting period to accomplish the goals?**
Nothing to report.

3) **IMPACT:**
a. **What was the impact on the development of the principal discipline(s) of the project?**Nothing to report
b. **What was the impact on other disciplines?**
Nothing to report
c. **What was the impact on technology transfer?**
Nothing to report
d. **What was the impact on society beyond science and technology?**
Nothing to report

4) **CHANGES/PROBLEMS:**
a. **Changes in approach and reasons for change**

i. *Describe any changes in approach during the reporting period and reasons for these changes. Remember that significant changes in objectives and scope require prior approval of the agency*

.

b. **Actual or anticipated problems or delays and actions or plans to resolve them**

As detailed in report from Oct 2017 our initial efforts in measuring behavioral performance on gap pre-pulse inhibition of acoustic startle (i.e., gap detection) tasks yielded mixed results in control and noise-exposed subjects. As a result, we reached out to Professor Alexander Galazyuk (Northeastern Ohio Medical College) for advice on the design of gap detection and behavioral assessment of tinnitus in mice. Professor Galazyuk has been forthcoming with advice and guidance in the redesign of our behavioral assessment workflow. His suggestions required a complete redesign of our behavioral paradigm, rebuilding of equipment, and changes to the associated analysis software. We then tested additional mice. We still failed to produce sufficient animals with behavioral evidence of tinnitus.

We also learned that the analysis of 2PLSM data for critical dynamics is much more difficult and time intensive than expected.

c. **Changes that had a significant impact on expenditures**

Nothing to report

Significant changes in use or care of human subjects, vertebrate animals, biohazards, and/or select agents Nothing to report

d. **Significant changes in use or care of human subjects**

e. **Significant changes in use or care of vertebrate animals.**

f. **Significant changes in use of biohazards and/or select agents**

5) **PRODUCTS:**

a. **Publications, conference papers, and presentations**

Report only the major publication(s) resulting from the work under this award.

i. **Journal publications.** *List peer-reviewed articles or papers appearing in scientific, technical, or professional journals. Identify for each publication: Author(s); title; journal; volume: year; page numbers; status of publication (published; accepted, awaiting publication; submitted, under review; other); acknowledgement of federal support (yes/no).*

We have performed additional experiments in control animals and extensive additional analysis to further understand population encoding of sounds. We found that the scale-free nature of the evoked activity enables persistent encoding of sound stimuli. This long-lasting effect might relate to the perception of tinnitus. If we obtain funding to continue, we will test this in future studies. We are working on a manuscript describing our results in control animals that will be submitted this month to *Cerebral Cortex*:

Z. Bowen*, D. E. Winkowski*, S. Seshradi, D. Plenz, P. O. Kanold; "Neuronal avalanches persistently encode transient sounds in input and associative layers of auditory cortex"
"Supported by NINDS U01NS090569 (POK, DP, WL), NIH RO1 DC009607 (POK), DOD W81XWH-16-1-0143 (POK, DW), and the Division of Intramural Research of the NIMH ZIAMH002797 (DP)."

We attached the current draft.

ii. **Books or other non-periodical, one-time publications.**

Nothing to report

iii. **Other publications, conference papers, and presentations.** *Identify any other publications, conference papers and/or presentations not reported above. Specify the status of the publication as noted above. List presentations made during the last year (international, national, local societies, military meetings, etc.). Use an asterisk (*) if presentation produced a manuscript.*

We have presented our results in control animals as non-refereed posters at 2 conferences:
D. E. Winkowski, Z. Bowen, S. Seshadri, D. Plenz, **P. O. Kanold**; "Critical Dynamics in A1 Networks During Sound Processing in the Awake Mouse", *Abstr. Assoc. for Res. in Otolaryngology* 2017

D. Winkowski, Z. Bowen, T.L. Ribeiro, D. Plenz, **P.O Kanold** "Reliable and persistent encoding of sounds across layers in the auditory cortex of awake mice", *Abstr. Soc. for Neuroscience* 2017

b. **Website(s) or other Internet site(s)**

N/A

c. **Technologies or techniques**.

N/A

Inventions, patent applications, and/or licenses

N/A.

Other Products

N/A.

6) **PARTICIPANTS & OTHER COLLABORATING ORGANIZATIONS**

a. **What individuals have worked on the project?**

i. *Provide the following information for: (1) PDs/PIs; and (2) each person who has worked at least one person month per year on the project during the reporting period, regardless of the source of compensation (a person month equals approximately 160 hours of effort). If information is unchanged from a previous submission, provide the name only and indicate "no change."*

Name:	*Patrick O. Kanold*
Project Role:	*PI*
Researcher Identifier (e.g. ORCID ID):	0000-0002-7529-5435
Nearest person month worked:	*1*
Contribution to Project:	*Dr. Kanold has overseen the project.*
Funding Support:	*unchanged*
Name:	*Daniel E. Winkowski*
Project Role:	*Co-PI*
Researcher Identifier (e.g. ORCID ID):	*0000-0003-4222-091X*
Nearest person month worked:	17
Contribution to Project:	*Dr. Winkowski has designed, implemented, and overseen all aspects of the project to date. Dr. Winkowski performed all imaging experiments and performed behavioral experiments and analysis.*
Funding Support:	
Name:	*James Narin*
Project Role:	*Technician*
Researcher Identifier (e.g. ORCID ID):	
Nearest person month worked:	*11*
Contribution to Project:	*Mr. Narin performed work in the area of behavioral testing of mice and hardware and software development.*
Funding Support:	

b. **Has there been a change in the active other support of the PD/PI(s) or senior/key personnel since the last reporting period?**

i. *If there is nothing significant to report during this reporting period, state "Nothing to Report."*

ii. If the active support has changed for the PD/PI(s) or senior/key personnel, then describe what the change has been. Changes may occur, for example, if a previously active grant has closed and/or if a previously pending grant is now active. Annotate this information so it is clear what has changed from the previous submission. Submission of other support information is not necessary for pending changes or for changes in the level of effort for active support reported previously. The awarding agency may require prior written approval if a change in active other support significantly impacts the effort on the project that is the subject of the project report.

Kanold is a Co-PI on an NIH U19 awarded in 9/2018. The goal of this grant is to develop and apply in vivo stimulation techniques to causally test the contribution of selected neurons to behavior.
Kanold is a Co-PI on an NIH R21 awarded in 9/2018. The goal of this grant is to develop automated behavioral and imaging systems for mice.,

There was no change in effort of Dr. Kanold in the grant performance period.

Dr. Winkowski applied for an NIH R21 to continue this work, but the application was unsuccessful.

c. **What other organizations were involved as partners?**
   1. **Organization Name:** Northeastern Ohio Medical College
   2. **Location of Organization:** *(if foreign location list country)* Rootstown, Ohio
   3. **Partner's contribution to the projec**t *(identify one or more)*
      a. **Financial support;** None
      b. **In-kind support** Partner has advised our group on establishing strategies for robust gap detection behavior for assessment of chronic tinnitus
      c. **Facilities** None
      d. **Collaboration** None
      e. **Personnel exchanges** None
      f. **Other.**

ci. **SPECIAL REPORTING REQUIREMENTS**

a. **COLLABORATIVE AWARDS:**

b. **QUAD CHARTS:**

cii. **APPENDICES:**

Neuronal avalanches persistently encode transient sounds in input and associative layers of auditory cortex

Zac Bowen[1,*], Daniel E. Winkowski[1,2,*], Saurav Seshradi[3], Dietmar Plenz[3], Patrick O. Kanold[1,2]

[1]Department of Biology, University of Maryland, College Park, MD 20742
[2]Institute for Systems Research, University of Maryland, College Park, MD 20742
[3]Section on Critical Brain Dynamics, National Institute of Mental Health, Bethesda, MD 20892

Key words: Auditory cortex, mouse, avalanche, pattern, memory

* These authors contributed equally

Corresponding author:
Patrick O. Kanold,
Dept. of Biology
University of Maryland
1116 Biosciences Res. Bldg.
College Park, MD 20742 USA

Abbreviated Title: Neuronal avalanches reliably and persistently encode sounds in A1

Conflict of interest: None

Acknowledgements & Contributions: DEW, DP and POK designed research. DEW performed experiments. ZB, DEW, and SS analyzed the data. ZB, DEW, SS, DP, and POK discussed the results and wrote the manuscript. The authors thank Dr. Karel Svoboda for sharing designs enabling awake imaging and Dr. Mark Andermann for advice on awake imaging and Dr. Wolfgang Losert for helpful discussions. Supported by NINDS U01NS090569 (POK, DP, WL), NIH RO1 DC009607 (POK), DOD W81XWH-16-1-0143 (POK, DEW), and the Division of Intramural Research of the NIMH ZIAMH002797 (DP). This study utilized the high-performance computational capabilities of the University of Maryland supercomputing resources (http://hpcc.umd.edu).

Abstract

The primary auditory cortex processes acoustic sequences for the perception of behaviorally meaningful sounds such as speech. Sound information arrives at its input layer 4 from where activity propagates to associative layer 2/3. The network activities that might allow both layers to process and maintain sound information over extended periods of times are currently not understood. Here, we identify common principles in sound processing for both layers that allow for the persistent encoding of sounds at the network level. Using *in vivo* 2-photon imaging of pyramidal neurons in mouse A1, we find that ensemble activity in cortical layers L4 and L2/3 separately exhibit neuronal avalanches characterized by similar power law relationships. Moreover, the temporal organization of avalanche activity, but not single neuron responses, reliably carries long-lasting mutual information in response to brief auditory stimuli that is independent of sound level. Our results demonstrate network principles linked to maximal dynamic range, optimal information transfer and matching complexity between L4 and L2/3 to shape population activity in auditory cortex. We suggest that the ability to encode brief tones over long periods of time in populations from both layers allows for the processing of complex acoustic sequences such as speech.

Introduction

Understanding speech or vocalizations depends on our ability to process sequences of sounds that vary over time in frequency and volume. The primary auditory cortex (A1) is central to encoding sound sequences (Nelken et al. 2003; Bartho et al. 2009; Francis et al. 2018), yet several major aspects of sound processing in A1 are currently not well understood. First, the selectivity of single A1 neurons to stimulus features such as sound frequency changes with sound level, i.e. across the dynamic range, while perceptual discrimination performance is largely level-invariant (Jesteadt et al. 1977; Wier et al. 1977; Bernstein et al. 2006). Second, responses of A1 neurons can be unreliable over repeated trials despite robust behavioral outcome (Deweese et al. 2004). Third, to successfully parse sound sequences, the identities of past sounds are relevant for the processing of current sounds. Accordingly, information about past stimuli should be available at the moment of sound perception, yet it is unclear whether and how such information is provided in A1. It was recently shown that auditory stimuli are encoded by populations of A1 neurons (Bathellier et al. 2012; Francis *et al.* 2018). Here, we hypothesize that reliable encoding of current and past sounds independently of sound level might be achieved at the neuronal population level.

Identifying population dynamics central to sound processing needs to take into account that A1 is composed of several cortical layers each transforming incoming information (Atencio and Schreiner 2009; Atencio, Sharpee, et al. 2009). Specifically, sensory inputs arriving in layer 4 (L4) are relayed to layers 2/3 (L2/3) via divergent and heterogeneous feed-forward projections (Meng et al. 2017). In this hierarchy, it is not well understood how population dynamics in L4 contributes to neuronal responses in L2/3 raising the general question of how neural representations of sensory stimuli are reliably transmitted through multilayer networks. At least two lines of evidence suggest that ensemble dynamics could support level-independent reliable sound encoding across networks of neurons. First, network dynamics that support a large dynamic range, i.e. that differentiate sounds at both high and low levels, should be of particular interest to auditory processing where sound amplitude can vary over many orders of magnitude. Simulations (Kinouchi et al. 2006; Shriki et al. 2016) and experiments *in vivo* (Gautam et al. 2015) and *in vitro* (Shew et al. 2009; Shew et al. 2010; Shew et al. 2011;

Shew et al. 2013) have shown that cortical networks that display neuronal avalanches (Beggs et al. 2003; Petermann et al. 2009; Shriki et al. 2013; Bellay et al. 2015) maximize their dynamic range for input processing as well as their information capacity (for review see (Chialvo 2010; Shew and Plenz 2013)). Neuronal avalanches are identified by power law relationships for the size and duration of activity in neuronal groups which naturally links to a second line of evidence identifying conditions for which information transmission between complex networks is maximized. Theory suggests that complex networks exchange maximal information if their complexity, quantified by their respective power law relationships, is matched (West et al. 2008; Aquino et al. 2010; Aquino et al. 2011). Accordingly, we hypothesize that if A1 population dynamics are governed by avalanche statistics, these statistics would be similar for L4 and L2/3.

Here, we identify common dynamical principles in sound encoding for both layers that allow for the persistent encoding of sounds in neuronal populations in line with predictions for neuronal avalanches. Using *in vivo* 2-photon imaging of pyramidal neurons in mouse A1, we demonstrate that brief sound stimuli induce long-lasting changes in the ensemble correlations such that ongoing activity in A1 carries information about past sounds.

Methods

All procedures were approved by the University of Maryland Institutional Animal Care and Use Committee. Mice were housed under a reversed 12 h-light/12 h-dark light cycle with ad libitum access to food and water. Imaging experiments were generally performed near the end of the light and beginning of the dark cycle. Age range at the time of experiments extended from P46-P100 (75 ± 21 days, mean ± std). Mice of both sexes were used (n=12, 8 Male, 4 Female) based on their availability not by any biased selection.

Animals:

Mice used for this study expressed the genetically encoded calcium indicator (GCaMP6s) (Chen et al., 2013). GCaMP6s was introduced in one of the following ways.

In a first line of experiments, we injected an adeno-associated virus (AAV1) into primary auditory cortex (A1) of C57/BL6 mice (n=5) for delivery of a calcium indicator with co-expression of a structural marker mRuby2 (Rose et al. 2016). Both proteins were under control of the synapsin promoter. Virus (AAV1.hSyn1.mRuby2.GSG.P2A.GCaMP6s.WPRE.SV40; titer: $3x10^{13}$) was obtained from the University of Pennsylvania Vector Core. Observed expression in these mice was primarily limited to supragranular and infragranular layers and was mostly absent in L4. Only data acquired from L2/3 in these animals was included. In a second line of experiments, we used transgenic mice that expressed GCaMP6s either under the Thy1 promoter (Dana et al., 2014, Jax: 024274, GP4.3) or a transgenic mouse line that conditionally expresses GCaMP6s when crossed to a mouse driver line expressing Cre recombinase under the control of Emx1 (Gorski et al., 2002; Madisen et al., 2015, GCaMP6s mouse: Jax: 024115; Emx1-Cre mouse: Jax: 005628). Both L2/3 and L4 datasets were acquired from the transgenic mice. The transgenic L2/3 and L4 data sets were always obtained sequentially in the same mouse, meaning the experiment (sound presentations) was conducted in one layer and then sequentially conducted in the other layer. The two transgenic lines exhibited robust indicator expression in both L4 and L2/3. We found no significant differences of indicator expression within layers when we compared across transgenic mouse lines and animals with viral expression and thus combined the data from different sources according to laminar position.

Surgery and animal preparation

Mice were given a subcutaneous injection of dexamethasone (5mg/kg) at least 2 hours prior to surgery to reduce potential inflammation and edema from surgery. Mice were deeply anesthetized using isoflurane (5% induction, 2% for maintenance) and given subcutaneous injections of atropine (0.2 mg/kg) and cefazolin (500 mg/kg). Internal body temperature was maintained at 37.5 °C using a feedback-controlled heating blanket. The scalp fur was trimmed using scissors and any remaining fur was removed using Nair. The scalp was disinfected with alternating swabs of 70% ethanol and betadine. A patch of skin was removed, the underlying bone was cleared of connective tissue using a bone curette, the temporal muscle was detached from the skull and

pushed aside, and the skull was thoroughly cleaned and dried. A thin layer of cyanoacrylate glue (VetBond) adhesive was applied to the exposed skull surface and a custom machined titanium head plate (based on the design described in Guo et al. (2014) was affixed to the skull overlying the auditory cortex using VetBond followed by dental acrylic (C&B Metabond). A circular craniotomy (~3 mm diameter) was made in the center opening of the head plate and the patch of bone was removed. For wild-type mice, virus (AAV1-syn-mRuby2-GC6s) was loaded into beveled glass pipettes and injected slowly into the areas corresponding to primary auditory cortex in 3-5 sites (~30 nL/site; ~250 – 300 μm from the surface; ~2 – 3 minutes/each injection site). Pipettes were left in place for at least 5 minutes after completion of each injection to prevent backflow. Then, a chronic imaging window was implanted. The window consisted of a stack of 2 – 3 mm diameter coverslips glued with optical adhesive (Norland 71, Edmund Optics) to a 5 mm diameter coverslip. The edges of the window between the glass and the skull were sealed with a silicone elastomer (Kwik-Sil) and then covered with dental acrylic. The entire implant except for the imaging window was then coated with black dental cement created by mixing standard white powder (Dentsply) with iron oxide powder (AlphaChemical, 3:1 ratio) (Goldey et al. 2014). Meloxicam (0.5 mg/kg) and a supplemental dose of dexamethasone were provided subcutaneously as a post-operative analgesic. Animals were allowed to recover for at least 1 week prior to the beginning of experiments.

Acoustic stimulation

Sound stimuli were synthesized in MATLAB using custom software (courtesy of P. Watkins, UMD), passed through a multifunction processor (RX6, TDT), attenuated (PA5, Programmable Attenuator), and delivered via ES1 speaker placed ~5 cm directly in front of the mouse. The sound system was calibrated between 2.5 and 80 kHz and showed a flat (±3 dB) spectrum over this range. Overall sound pressure level (SPL) at 0 dB attenuation was ~90 dB SPL (for tones). Sounds were played at three sound levels (40, 60, and 80 dB SPL). Auditory stimuli consisted of sinusoidal amplitude-modulated (SAM) tones (20 Hz modulation, cosine phase), ranging from 3 – 48 kHz. For wide-field imaging, the frequency resolution of the stimuli was 1 tone/octave; for 2-photon imaging,

the frequency resolution was 2 tones/octave (0.5 octave spacing). Each of these tonal stimuli was repeated 5 times with a 4 – 6 s interstimulus interval for a total of either 75 (wide-field) or 135 (2-photon) iterations.

Wide-field imaging

In order to construct sound-evoked response maps using wide-field imaging, awake mice were placed into a plastic tube with a head restraint system similar to that described by Guo et al. (2014). Blue excitation light was provided by an LED (470 nm, Thorlabs) or xenon-arc lamp (Lambda LS, Sutter Instruments) equipped with an excitation filter (470 nm CWL, 40 nm FWHM; Chroma ET470/40x) and directed toward the cranial window. Emitted light was collected through a tandem lens combination (Ratzlaff et al. 1991) consisting of a 55 mm lens and 85 mm lens affixed to the camera and passed through a longpass (495 nm cutoff, Chroma Q495lp) followed by a bandpass emission filter (525 nm CWL; 50 nm FWHM; Chroma HQ525/50). Images were acquired using StreamPix software (NorPix) controlling a CoolSNAP HQ2 CCD camera (Photometrics). After acquiring an image of the surface vasculature, the focal plane was advanced to a depth corresponding to ~300 – 400 μm below the brain surface. One trial of stimulation consisted of ~1 – 2 s of quiet, followed by sound onset (3 – 48 kHz frequency; 1 octave spacing; 1 s duration; 20 Hz modulation rate; 40, 60, 80 dB SPL) then 1 – 2 s of quiet. Each frequency-level combination was randomly repeated 5 times for a total of 75 iterations. Inter-trial interval was ~10 – 15 s. Acquisition of each frame was individually triggered and synchronized with the sound presentation using the Ephus software suite (http://www.ephus.org) (Suter et al. 2010).

2-photon imaging

To study cellular neuronal activity using 2-photon imaging, we used a scanning microscope (Bergamo II series, B248, Thorlabs) coupled to a pulsed femtosecond Ti:Sapphire 2-photon laser with dispersion compensation (Vision S, Coherent). The microscope was controlled by ThorImageLS software. The laser was tuned to a wavelength of λ = 940 nm in order to simultaneously excite GCaMP6s and mRuby2.

Red and green signals were collected through a 16× 0.8 NA microscope objective (Nikon). Emitted photons were directed through 525/50-25 (green) and 607/70-25 (red) band pass filters onto GaAsP photomultiplier tubes. The field of view was 370x370 μm^2. Imaging frames of 512×512 pixels (0.52 μm^2 pixel size) were acquired at 30 Hz by bi-directional scanning of an 8 kHz resonant scanner. Beam turnarounds at the edges of the image were blanked with a Pockels cell. The average power for imaging in both L2/3 and L4 was <~70 mW, measured at the sample plane.

Data Analysis

Wide-field image sequences were analyzed using custom routines written in Matlab (Mathworks). Images were parsed into trial-based epochs in which each frame sequence represented a single trial consisting of the presentation of a single sound frequency-intensity combination. For each trial, response amplitude ($\Delta F/F_0$) as a function of time was determined for each pixel using the formula $((F - F_0)/ F_0)$ where F corresponds to the time varying fluorescence signal at a given pixel and F_0 was estimated by averaging the fluorescence values over 4 frames (~1 s) prior to sound onset for a given trial and pixel. For construction of sound-evoked response maps, the amplitude of the $\Delta F/F_0$ pixel response during 1 s after stimulus onset (~4 frames) was averaged across time and repetitions yielding an average response magnitude that was assigned to each pixel. Responsive areas in the average response maps were defined on a pixel-by-pixel basis as pixels in which the average brightness of the pixel during the 1 s after stimulus onset exceeded 2 standard deviations of the pixel brightness during the 1 s before the stimulus across stimulus repetitions.

2-photon image analysis

Image sequences were corrected for x-y drifts and movement artifacts using either the TurboReg in ImageJ (Thevenaz et al. 1998; Schindelin et al. 2012) or discrete Fourier transform registration (Guizar-Sicairos et al. 2008) implemented in Matlab (Mathworks) taking advantage of mRuby2 labeled neurons. Neurons were identified manually from the average image of the motion corrected sequence. Ring-like regions of interest (ROI) boundaries were drawn based on the method described in Chen et al. (Chen et al.

2013). Overlapping ROI pixels (due to closely juxtaposed neurons) were excluded from analysis. For each labeled neuron, a raw fluorescence signal over time (F) was extracted from the ROI overlying the soma. The mean fluorescence for each neuron was calculated across frames and converted to a relative fluorescence measure ($\Delta F/F_0$), where $\Delta F = (F - F_0)$. F_0 was estimated by using a sliding window that calculated the average fluorescence of points less than the 50^{th} percentile during the previous 10-second window (300 frames). Neuropil (NP) subtraction was performed on all soma ROIs (Peron et al. 2015). In short, the neuropil ROI was drawn based on the outer boundary of the soma ROI and extended from 1 pixel beyond the soma ROI outer boundary to 15 μm excluding any pixels assigned to neighboring somata. Thus, the final $\Delta F/F_0$ used for analysis was calculated as $\Delta F/F_0 = (\Delta F/F_0)_{soma} - (\alpha \times (\Delta F/F_0)_{NP})$, where we used $\alpha = 0.9$ (Peron *et al.* 2015) to reduce fluorescence contamination from the neuropil. Neurons in which the $\Delta F/F_0$ signal was significantly modulated by sound presentation were defined by ANOVA ($p < 0.01$) across baseline (pre-stimulus) and all sound presentation periods. Single neuron receptive fields (sRF) were determined as the average $\Delta F/F_0$ response to each frequency-intensity combination across 5 stimulus repetitions during the stimulus window (1 s). Best frequency (BF) for sRFs was determined as the center of mass of the responses across all stimuli. In order to distinguish tuned and untuned cells, the cell's average $\Delta F/F_0$ from each individual trial was compared across all frequency-intensity combinations. ANOVA ($p<0.01$) was used to determine if the mean responses to a frequency-intensity combination differed from the rest of the stimuli, thus deeming the cell tuned.

Neuronal ensemble and avalanche analysis

Deconvolution of neuropil-corrected $\Delta F/F_0$ traces was performed using the Suite2P implementation of OASIS without an L1 penalty (Pachitariu 2017). This transformation yields a spike probability estimate (λ) for each pyramidal neuron and frame. The time course of λ for each neuron was combined into a spike raster plot, which depicts the probability of spiking for each neuron and each frame. Using a simple threshold (λ_{thr}), neurons above λ_{thr} were deemed active and neurons below λ_{thr} were deemed inactive for each imaging frame. Accordingly, the thresholded spike raster plots were binarized,

with active neurons set to the value 1 and inactivity neurons set to the value 0 for each frame. We note that the specific value of λ_{thr} is a free parameter, which determines the number of spatiotemporal activity clusters chosen (see below). If λ_{thr} is very low, most neurons are deemed active all the time, resulting in a small number of very large activity clusters. Conversely, if λ_{thr} is very high, most neurons are considered inactive, again reducing the number of activity clusters. Accordingly, we calculated the number of activity clusters for a range of λ_{thr} using 100 logarithmically-spaced values from the minimum inferred spike value (λ_{min}) to the maximum inferred spike value (λ_{max}). The λ_{thr} chosen for each data set maximized the number of activity clusters (see below)(see (Bellay *et al.* 2015).

Activity clusters were defined based on contiguous frames in which at least 1 neuron was active (see also Figure 2b) (Bellay *et al.* 2015). Thus, activity clusters are bounded by periods of silence in the population activity. Clusters typically contained a varying number of active pyramidal neurons which could be active for only one or numerous frames within a cluster. The cluster size was defined as the number of neurons active in a cluster summed over the number of frames each neuron was active. Cluster duration, also called cluster lifetime was defined as the number of frames constituting a cluster. For analysis, clusters were assigned to the temporal window when they initiated. For example, a cluster that initiated during the 1 s stimulus window ($Stim_{on}$), even when it continued after stimulus offset, was categorized as a $Stim_{on}$ cluster.

To test if activity clusters exhibit statistical properties of neuronal avalanches, we analyzed the probability distributions of both cluster size and cluster duration. First, the distributions for both cluster size and duration were binned logarithmically, and probability density functions were obtained. For both the size and duration, we fit a power law or exponential distribution. We compared these fits and estimated parameters by calculating the log-likelihood ratio (LLR) by likelihood maximization as described previously (Clauset et al. 2009; Klaus et al. 2011). Slopes of the power law distributions (alpha values) were obtained using Kolmogorov-Smirnov goodness-of-fit to minimize the KS distance between the empirical distribution and a theoretical distribution for a range of alpha values (Clauset *et al.* 2009; Klaus *et al.* 2011). For

controls, shuffled cluster distributions were calculated from shuffled rasters using the same analysis outlined above. For shuffled rasters, each neuron separately had its spike probability estimates randomly permuted in time. This means the per-frame spike probabilities were maintained for each neuron, therefore maintaining the total number of active frames for each neuron. However, the individual temporal shuffling of neurons abolishes any temporal correlations between neurons. The shuffling process was repeated 10 times.

Pairwise cross-correlation analysis was computed using zero-lag correlation of the λ estimates for all active neurons across the entire imaging session.

Mutual information analysis

Stimulus encoding matrices were produced as follows. For each activity cluster, a cluster receptive field (cRF) was computed from a weighted average of the sRFs of n neurons participating in the cluster. The average was weighted by including neuronal sRFs according to how many frames f they were active (nonzero lambda) within the cluster.

$$cRF = \frac{\sum_{i=1}^{n} f_i \, sRF_i}{\sum_{i=1}^{n} f_i}$$

These cRFs were then organized into a two-dimensional histogram according to the frequency and sound level of the presented stimulus (see also Figure 4)

Mutual information $I(S;R)$ was calculated on the stimulus encoding matrices as follows:

$$I(S;R) = \sum_{s,r} P(r,s) \log_2 \frac{P(r,s)}{P(r)P(s)}$$

where P(s) is the probability of presenting stimulus s, P(r) is the probability of observing neural response r across all trials of all stimuli, and P(r,s) is the joint probability of observing response r when stimulus s is presented. Mutual information was calculated on the 2D histograms of stimulus presented versus observed cluster RFs. Marginal and joint probabilities were obtained from the observed values in the 2D histogram. To eliminate bias of the tuning distribution in the field of view (FOV), true MI values were

compared to MI values of surrogate datasets (Schreiber et al. 2000). The surrogate dataset was produced by using the marginal probabilities of the 2D histogram in the real dataset to generate a new (surrogate) 2D-histogram while maintaining the same total number of data points. This process was repeated for 100 surrogates and then the mean and standard deviation were computed. The MI values reported in bits are the difference between the real data MI value and the mean surrogate MI value with error bars representing the standard deviation of the surrogate MI values. The theoretical maximum MI occurs when the stimuli can be perfectly inferred from the neuronal activity (Quian Quiroga et al. 2009). In this case the 2D histogram would be represented by an identity matrix where the mutual information equation above reduces to $I(S;R) = H(S) = \log_2(9)=3.17$ bits. This maximum is unattainable from our data as it would require that each neuron is perfectly tuned to a single stimulus and only became active during that stimulus. The MI ratio was computed by dividing the real data MI values by the MI values produced from the shuffled avalanche distributions. A ratio equal to 1 would indicate that the temporal structure of the real data does not contain significant information about the stimulus.

Neuronal population pruning was performed by omitting one cell from the raster and performing the neuronal avalanche analysis and mutual information analysis outlined above. This was iterated to omit additional cells up to 75% of the cell population excluded with a lower limit of at least 10 cells included in the analysis. Cells were left out according to their mean spike rate over the entire imaging session with the most highly active cells left out first, regardless of their responses to sound stimuli. The lower limit used in the population pruning analysis is due to statistical limitations of computing MI from single cells or a very low number of cells. For example, computing the MI from a single cell would leave much of the stimulus encoding matrix empty on stimuli where the neuron did not respond. Furthermore, the stimuli with responses from that single cell would have identical columns in the matrix.

Results

To compare responses of single neurons and neuronal ensembles, i.e. groups of groups, to auditory stimuli, we used *in vivo* 2-photon intracellular calcium imaging to

sequentially measure activity of primarily pyramidal neurons expressing GCaMP6s in layer 2/3 (L2/3) and layer 4 (L4) in awake mice (n = 12 mice; Fig. 1a). Throughout the experiment the awake animal rested under the microscope while listening passively to semi-random presentation of 1 s short tonal sounds at 8 frequencies (3 – 48 kHz) and 3 different sound pressure levels (40, 60, 80 dB) separated by 4 – 6 s. Each stimulus was repeated 5 times over the course of the experiment. We identified primary auditory cortex (A1) using widefield imaging (Fig. 1b). We then imaged the activity of neurons in L4 and L2/3 by imaging in different focal planes (Fig. 1c, d). For each neuron an instantaneous spike probability (λ) over time was obtained from the time varying calcium signal using spike deconvolution from Suite2P (Pachitariu 2017) (see also Fig. 2a). Continuous time courses of λ were thresholded for $\lambda > \lambda_{thr}$ (see Material and Methods) to identify frames during which neurons fired action potentials.

To assess neuronal variability without external stimuli, we first analyzed ongoing activity in the absence of sound presentation. Ongoing activity was largely similar in both layers. Average λ was close to $\lambda = 0.05$ per frame, which translates into ~ 1.5 spikes/s at a frame rate of 30 frames/s (L4: 0.060 ± 0.037; L2/3: 0.061 ± 0.036; $p>0.84$). As indicated by CVs between 1 – 2, highly irregular firing dominated both L4 and L2/3 with most irregular firing found in L4 neurons (Fig. 1e, f). Despite this irregularity, the distributions of pairwise cross-correlation were heavy-tailed with higher correlations found in L2/3 (Fig. 1g). These positive correlations indicate that neurons share common input and/or interact over distances during ongoing activity. These results are consistent with *in vitro* studies showing common inputs and connections in L2/3 of A1 (Oswald et al. 2009; Levy et al. 2012; Watkins et al. 2014; Meng *et al.* 2017).

Ongoing ensemble activity in A1 organizes as neuronal avalanches

To better understand the organization of neuronal ensemble activity, we grouped neurons based on the temporal association of their firing with other neuronal firings irrespective of spatial location, which is known to show functional heterogeneity in auditory and visual cortex (Ohki et al. 2005; Bandyopadhyay et al. 2010; Rothschild et al. 2010; Martin et al. 2013; Winkowski et al. 2013). We first identified active neurons in the imaging field from the inferred spike raster by setting each $\lambda > \lambda_{thr}$ to 1 and $\lambda < \lambda_{thr}$ to

0 (binarized raster; Fig. 2a). We then defined an activity cluster as an ensemble of neurons that was active over successive imaging frames. Each activity cluster was bound by time intervals that did not contain any active neuron, i.e. they exhibited successive time intervals in which at least 1 neuron was active (Fig. 2b; see also Material and Methods). The numbers of active neurons could vary between time bins with some neurons being active in certain bins while others were active at other bins. Thus, activity clusters could range from very small, e.g. a single neuron firing once to large e.g. many neurons firing over many imaging frames. We then characterized these activity clusters by measuring their size and duration. We quantified the size of each cluster by adding its corresponding numbers of spikes for each active neuron in each time bin and calculated the probability density function of cluster sizes (Fig. 2c). Qualitative inspection showed a high probability of occurrence of small clusters and a smaller probability of occurrence of very large clusters. The probability distribution appeared linear in a logarithmic plot suggestive of a power-law distribution. Indeed, the probability density distributions of cluster size were significantly better fit by a power law with slope close to -2 compared to an exponential function (Fig. 2c, e, LLR_{L4} = 480.0 to 1251.9; $LLR_{L2/3}$ = 551.8 to 1243.8; $p<10^{-13}$; FOV_{L4} = 9; $FOV_{L2/3}$ = 10). These power laws were abolished by temporal shuffling (see Methods; Fig. 2c; $LLR_{L4\text{-}shuff}$ = -690.9 to -175.1; $LLR_{L2/3\text{-}shuff}$ = -424.9 to -108.8; $p<10^{-8}$, favors exponential over power law) indicating that the temporal structure of the ensemble activity is important in imparting the power law distribution of the activity cluster size. We next quantified the temporal duration of each activity cluster, which is the number of consecutive time bins for each cluster. The distribution of cluster duration also obeyed a power-law distribution (Fig. 2d, e, LLR_{L4} = 353.9 to 796.7; $LLR_{L2/3}$ = 381.8 to 849.9; $p<10^{-34}$), which was once again abolished by temporal shuffling (see Methods; Fig. 2d; $LLR_{L4\text{-}shuff}$ = 232.3 to 586.4; $LLR_{L2/3\text{-}shuff}$ = 57.2 to 459.4; $p<0.01$, favors exponential over power law). The presence of power-law distributions for cluster size and duration suggests that ongoing activity in L4 and L2/3 organizes as scale-invariant neuronal avalanches similar to ongoing activity in other cortical regions (Bellay *et al.* 2015). These results suggest that the network is poised to process incoming sensory stimuli with maximal dynamic range (Kinouchi and Copelli 2006).

Evoked ensemble activity in A1 organizes as neuronal avalanches

We next investigated how the presence of a sound stimulus alters the ensemble activity in A1. During an auditory stimulus, more A1 neurons fire and are thus recruited into ongoing active ensembles. Accordingly, sound evoked ensemble activity could deviate from this stable avalanche regime for example by selectively increasing the numbers of large clusters. Alternatively, sound evoked A1 ensemble activity could maintain scale-invariant organization by increasing clusters of all sizes. Across the presentation of all stimuli, overall firing rates remained low in both layers (L4: 0.066 ± 0.032; L2/3: 0.056 ± 0.020; $p<10^{-8}$). As expected, short tonal sounds transiently increased neuronal ensemble activity in A1 after which firing returned to baseline in both L4 and L2/3 (Fig. 3a, b). We next characterized the sound evoked ensemble activity. From the event structure, we defined $Stim_{On}$ clusters as activity clusters initiated during the 1 s of sound presentation and $Stim_{Off}$ clusters as activity clusters initiated following sound offset (Fig. 3c). We then characterized separately the size and duration (lifetime) of the $Stim_{On}$ clusters and $Stim_{Off}$ clusters. Consistent with the increase in activity of single neurons by sound stimulation, the average size and lifetime of $Stim_{On}$ clusters increased systematically with sound level (i.e., input strength) (Fig. 3d, S1). Importantly, $Stim_{On}$ clusters of L4 and L2/3 remained power-law distributed in both size and lifetime (Fig. 3d, Supplemental Table 1, 2). Consistent with neuronal activity returning to spontaneous levels after sound presentation (Fig. 3a, b), neither the average size and lifetime of $Stim_{Off}$ clusters changed with sound level (Fig. 3d, S1) and nor did their corresponding distributions deviate from a power law (Fig. 3d, Supplemental Table 1, 2). Thus, scale-invariant avalanche dynamics in both layers L4 and L2/3 are preserved even in the presence of distinct sound input to A1 and across different sound amplitudes. Moreover, reverberating population activity after sound offset maintained avalanche organization independent of the level of the preceding sound.

Ensemble activity carries stimulus information independent of sound level and beyond stimulus presentation

Having identified population dynamics that are sound level invariant, we then studied the encoding of stimulus information for single neurons and ensembles. First, we characterized single neuron receptive fields (sRF) and demonstrated their dependency on sound level. Many neurons recorded in each layer were responsive to sound, i.e. showed an increase in firing during $Stim_{on}$. In figure 4a, we provide three examples of sRFs from A1 quantifying the change in stimulus specificity as a function of sound level. Stimulus specificity was found to broaden with an increase in sound volume (Fig. 4a, left), to exist only at a particular sound level (Fig. 4a, middle), or to broaden with a decrease in sound volume (Fig. 4a, right). Simultaneously imaged neurons in both layers did show heterogeneity of tuning in their responses (Fig. 4a) and this heterogeneity has been previously reported to be larger in L2/3 than L4 (Bandyopadhyay *et al.* 2010; Rothschild *et al.* 2010; Winkowski and Kanold 2013; Maor et al. 2016).

Given this local tuning heterogeneity of the imaged population, we thus asked whether ensemble activity carries robust information about the presented stimulus. Specifically, we determined whether stimulus preferences, typically calculated for single neurons, also emerge at the population level in L4 and L2/3. In a first step, we assessed stimulus preference of the activated population of neurons for 1 s periods during $Stim_{On}$ and $Stim_{Off}$ conditions. The cluster receptive field (cRF) was computed as the average of the sRF of the active neurons weighted according to the number of inferred spikes produced by each neuron in the activity cluster (Fig. 4b). We note that inferred activity of untuned neurons, which did not demonstrate any selectivity for the presented stimuli (see Methods), was included in our calculations of the cRF. For each sound level, the average tuning profile was entered into a 2D histogram in which each column corresponded to the presented tone (Fig 4c, *top*) and repeated for each sound stimulus resulting in a confusion matrix for 1 s of $Stim_{On}$ and corresponding 2 s of $Stim_{Off}$ population activity (Fig. 4c, *bottom*). If the population tuning profile at a given sound level reliably identified the presented stimulus frequency at that level, then the maximum count in the confusion matrix was on the diagonal. In contrast, off diagonal counts indicated non-matched responses. We found that the relationship of the cRF and the

presented sound stimulus in both layers showed diagonality (Fig. 4d; $Stim_{On}$) indicating a systematic relationship between presented stimulus and cRF.

To quantify these observations, we calculated the mutual information (MI) of the confusion matrix for each layer, $Stim_{On}$ and $Stim_{Off}$ periods and sound level (Fig. 4e; see Material and Methods). As expected for a primary sensory cortex, we found that active populations had MI greater than chance for each experiment in both layers and for all sound levels during the stimulus (Fig. 4e; Supplemental Table 3). Average MI was similar in both layers and independent of sound level ($p > 0.19$, Fig. 4f) indicating that stimulus information is encoded in both L4 and L2/3 over a wide dynamic range. Similar results in both layers suggest that there is no loss of information during cortical processing of sound from L4 to L2/3. These MI values are consistent with MI values observed using electrophysiological measures (Klampfl et al. 2012; Petrus et al. 2014).

Selectively tuned neurons and population temporal correlations are essential for persistent stimulus encoding

Our finding that MI between active populations and the stimulus remained high during $Stim_{Off}$ despite average firing rates returning to pre-stimulus conditions prompted us to study the temporal evolution of population MI and its relationship with single neuron firing rates. As a control, we compared original MI values (MI_{data}) to those obtained from shuffled temporal responses ($MI_{shuffled}$) and compared the ratio between the two. We found that this ratio was significantly larger than 1 in both layers even for population activity up to 3 s after the stimulus had ended (Fig. 5a), indicating that the temporal correlations between neurons are important for carrying stimulus information.

Our analysis so far has included all neurons, including those that did not show any obvious frequency preference. Prior studies suggested that “untuned” neurons might contribute to measured MI (Zylberberg 2017). We assessed this possibility by separating the population into tuned neurons and untuned neurons and recomputing the MI using sRFs from one group at a time. As expected, we found that when the MI analysis is performed computing cRFs only from tuned neurons we find that MI is significantly higher compared to when the analysis is performed using only untuned neurons. In general, tuned neurons carried significantly more MI than untuned neurons

for longer duration and higher sound volume (Fig. 5b). This demonstrates that our approach to identify significant MI ratios at the cluster level properly incorporates single neuron tuning. On the other hand, untuned neurons still contributed a significant amount of MI to the total population response (Fig. 5b).

Stimulus information is primarily carried by the most active neurons in stimulus-evoked and post-stimulus population activity in A1

To investigate whether single neurons were representing most of the stimulus information in the population or if the information was distributed among the population, we carried out an exclusionary analysis and recomputed the MI. Each neuron's average firing rate across the entire experiment was used as the exclusion criteria. This provided an unbiased property of each neuron as it was averaged across all stimuli presented during the experiment. We sequentially excluded the most active neurons one at a time from the population raster, repeated the full avalanche analysis, and re-calculated the MI ratio. We found that for both layers L4 and L2/3, MI was carried by the most active neurons during all temporal windows as indicated by a corresponding decrease in MI with successive removal of the most active neurons over all sound levels (Fig. 6a, b; Supplemental Table 4). However, some information about the stimulus was retained even with successive removal of the majority of highly active neurons indicating that the stimulus information is distributed among the population rather than contained in just the most active cells.

Discussion

We identified several fundamental properties of how A1 reliably represents stimuli in its spatiotemporal population response. First, we demonstrated that A1 represents even simple sound stimuli as temporally varying activity across distributed populations of diversely tuned pyramidal neurons. Second, pyramidal group activity in both layers obey similar statistical laws in that the size and duration of ongoing and sound evoked activity clusters shows scale-invariance, the hallmark of neuronal avalanches. Finally, by introducing a novel approach of cluster tuning (cRFs), we demonstrated that cluster activity carried information about a preceding stimulus even

though the firing rates of individual neurons had decayed to pre-stimulus levels. This finding clearly demonstrates that reverberant ongoing ensemble activity in A1 exhibits long-range temporal correlations essential to encode stimulus information.

Our finding that both ongoing and evoked activities show signatures of neuronal avalanches is in line with experiment and theory associating avalanches with the optimization of numerous aspects of information processing such as dynamic range, information processing and transmission within layers (Shew *et al.* 2009; Shew *et al.* 2010; Shew *et al.* 2011; Shew and Plenz 2013; Gautam *et al.* 2015) and between layers (West *et al.* 2008; Aquino *et al.* 2010; Aquino *et al.* 2011). That avalanche organization is maintained during as well as after stimulus presentation extends previous findings in *ex vivo* turtle visual cortex based on the local field potential demonstrating a return to avalanche organization after visual stimulation (Shew et al. 2015; Clawson et al. 2017). The selective labeling of pyramidal groups in our experiments also specifically links avalanche dynamics to pyramidal groups, thereby extending previous reports on evoked avalanches in mice using a non-selective bulk labeling approach (Karimipanah et al. 2017). In summary, our work firmly suggests that A1 networks across layers and stimulus presentation optimize transmission of sound information by maintaining neuronal avalanche organization.

The reported statistics of neuronal clusters is sensitive to sampling conditions. Spatial subsampling, in which only a small percentage of the population is measured, will change an expected power law distribution to an exponential form, an effect clearly visible at subsampling below 10% or more as shown in simulations (Priesemann et al. 2009; Ribeiro et al. 2010; Ribeiro et al. 2014; Levina et al. 2017). Subsampling might be the main reason why avalanches have not been observed in spike recordings using microelectrode arrays representing much lower subsampling conditions (Petermann *et al.* 2009; Ribeiro *et al.* 2010; Touboul et al. 2010). 2-photon imaging at cellular resolution allows for much higher neuronal sampling conditions and has been used previously to identify neuronal avalanches (Bellay *et al.* 2015; Seshadri et al. 2018) using non-negative deconvolution (Vogelstein et al. 2010). In the present study, we combined 2-photon imaging with an advanced, yet robust spike density estimation (Pachitariu et al. 2018) providing further support that spatiotemporal activity in spiking

pyramidal groups organizes as neuronal avalanches. We also note that spiking between pyramidal neurons is significantly correlated, excluding models for the generation of power laws that feature no interaction between neurons (Martinello et al. 2017; Touboul et al. 2017). Our findings of robust power laws even under non-stationary conditions, i.e. evoked responses, are in line with previous reports in non-human primates based on the local field potential (Yu et al. 2017). We conclude that 2-photon imaging of cortical layers at cellular resolution in combination with robust spike density estimates allows for the clear identification of scale-invariant activity in ongoing and evoked population activity in primary auditory cortex.

We also demonstrate that avalanche organization and the encoding of stimulus information is largely independent of sound level. This *in vivo* demonstration of a large dynamic range for A1 network activities matches reports on level-invariant perceptual discrimination performances (Jesteadt *et al.* 1977; Wier *et al.* 1977; Bernstein and Oxenham 2006). It suggests that population coding of sound information might underlie level-invariant performances.

Our finding that sound information distributes across tuned and untuned neurons in reverberant network activity long after cessation of the stimulus relates ongoing activity to stimulus evoked activity (Arieli et al. 1996; Luczak et al. 2009). Since critical systems obeying avalanche dynamics show long-range spatial and temporal correlations (Chialvo 2010), our results aid to unify these seemingly disparate activity states and suggest that ongoing activity reflects the history of past stimuli. Our controls demonstrate that both during stimulus and post-stimulus periods, untuned neurons carry lower information than tuned neurons, yet, their overall contribution to the mutual information of the stimulus is still above what would be expected from random activity. Optimal stimuli have been shown to evoke sustained responses in single A1 neurons during stimulus presentation (Wang et al. 2005; Wang 2007). In contrast, we observed stimulus information in the A1 ensembles even after stimulus cessation when the firing rates of individual neurons have returned to baseline levels. Thus, while A1 rapidly encodes sensory stimuli in large neuronal ensembles, a representation of the prior stimulus is maintained by modulating population relationships of the baseline activity of individual neurons. Prior reports demonstrated that A1 neurons carry information not

only about current tone stimulus but also the immediately preceding tone (~100ms) in a sequence of tonal stimuli (Klampfl *et al.* 2012). Our findings extend this window of maintained stimulus information by almost 2 orders of magnitude.

The weak dependence between the size of the neuronal population and MI long after stimulus offset demonstrates that, for both layers, information remains distributed over many neurons, more so in L4 than in L2/3. This finding suggests that after initial activation of specific L4 and L2/3 networks stimulus information is propagated and retained in diverse distributed networks as reverberant network activity. This persistent representation of the sound stimulus might influence processing of subsequent stimuli. Indeed, investigations of stimulus context-dependent processing in the auditory cortex of cats and primates demonstrate that preceding stimuli can influence single unit responses for up to 1 s (Brosch et al. 2000; Bartlett et al. 2005). Our findings of persistent stimulus information are consistent with this idea. Moreover, by extending the analysis to neuronal ensemble activity, we extend this window much further in time (several seconds) and the scale-free nature of neuronal avalanches suggest even longer time windows. Such multi-scale temporal integration is likely relevant in representing temporally complex stimuli (i.e., vocalizations) that contain features that change on the order of hundreds of milliseconds to seconds or for representing other situation-dependent communication signals. Importantly, our analyses suggest that not all of the stimulus information is encoded in the firing rate of individual neurons but rather by the distributed temporal activity relationships of many neurons. Processes that coordinate these activity relationships, e.g. inhibitory circuits or electrical synapses between neurons, might be poised to control the window of temporal integration. Our results further show that disruption of these temporal relationships of the neuronal ensembles abolishes the information encoding capability. Thus, subtle disruptions of network activity that may not cause changes of the firing rate of single neurons, nor cause hyperactivity of the network, can nevertheless alter network function.

In summary, our work reveals several key aspects of auditory cortical dynamics and in general cortical sensory coding. Even simple sensory stimuli are represented across distributed populations of diversely tuned neurons and the activated neuronal ensembles carry information beyond stimulus cessation by their ensemble activity

correlations. Thus, the relative timing of activity in neuronal ensembles is an important contributor to neuronal encoding.

Supplemental Tables

L2/3	Stim On High dB	Stim On Mid dB	Stim On Low dB	Stim Off High dB	Stim Off Mid dB	Stim Off Low dB
LLR Actual	2573.9	2448.7	2094.4	3356.6	5151.7	3332.0
Mean shuff	-0.3	14.2	3.6	36.2	20.9	31.7
std_\ shuff	40.1	50.6	47.1	68.7	57.8	69.8
Test	't-test'	't-test'	't-test'	't-test'	't-test'	't-test'
P-Value	5.90×10^{-181}	1.40×10^{-168}	3.66×10^{-165}	8.62×10^{-169}	6.91×10^{-195}	7.97×10^{-168}
L4	Stim On High dB	Stim On Mid dB	Stim On Low dB	Stim Off High dB	Stim Off Mid dB	Stim Off Low dB
LLR Actual	1357.4	1480.3	1213.9	1788.3	1851.7	1867.1
Mean_shuff	104.3	99.8	115.5	220.9	204.4	220.0
std_shuff	39.3	35.3	39.5	55.2	57.3	49.0
Test	't-test'	't-test'	't-test'	't-test'	't-test'	't-test'
P-Value	7.05×10^{-151}	1.19×10^{-159}	4.52×10^{-145}	6.38×10^{-146}	1.69×10^{-146}	3.29×10^{-153}

Supplemental Table 1. Statistical comparisons of the log-likelihood ratio values from actual avalanche size distributions obtained from spontaneous activity and shuffled avalanche size distributions.

L2/3	Stim On High dB	Stim On Mid dB	Stim On Low dB	Stim Off High dB	Stim Off Mid dB	Stim Off Low dB
LLR Actual	1361.4	1337.9	1246.8	2185.4	2176.1	2116.0
Mean shuff	356.8	381.0	360.9	743.6	736.2	738.4
Std shuff	36.6	41.5	42.0	50.1	49.7	54.8
Test	't-test'	't-test'	't-test'	't-test'	't-test'	't-test'
P-Value	1.56×10^{-144}	4.72×10^{-137}	3.25×10^{-133}	1.65×10^{-146}	8.82×10^{-147}	1.03×10^{-140}
L4	Stim On High dB	Stim On Mid dB	Stim On Low dB	Stim Off High dB	Stim Off Mid dB	Stim Off Low dB
LLR Actual	824.0	946.8	817.5	1313.8	1328.7	1350.6
Mean shuff	422.9	423.8	433.2	836.6	833.3	851.5
Std shuff	35.3	36.6	35.9	45.2	49.9	45.0
Test	't-test'	't-test'	't-test'	't-test'	't-test'	't-test'
P-Value	9.89×10^{-107}	1.75×10^{-116}	3.30×10^{-104}	1.45×10^{-103}	6.08×10^{-101}	1.29×10^{-105}

Supplemental Table 2. Statistical comparisons of the log-likelihood ratio values from actual avalanche lifetime distributions obtained from spontaneous activity and shuffled avalanche lifetime distributions.

Comparison p-values					
L2/3	Stim on	Stim off	**L4**	Stim on	Stim off
High - Mid	0.660	0.882	High - Mid	0.983	0.988
High - Low	0.783	0.998	High - Low	0.961	0.773
Mid - Low	0.977	0.910	Mid - Low	0.996	0.683
Test used	ANOVA	Kruskal-Wallis	Test used	Kruskal-Wallis	Kruskal-Wallis

Supplemental Table 3. Statistical comparison of MI values at each sound level. MI values did not significantly differ between sound levels. Each distribution was checked for normality and then a multiple comparison test was used as noted.

Linear regression slopes

L2/3	Stim on	Stim off 1	Stim off 2	Stim off 3
High dB	-0.079	-0.063	-0.029	-0.093
Mid dB	-0.101	-0.049	-0.052	-0.088
Low dB	-0.053	-0.033	-0.046	-0.051
L4	Stim on	Stim off 1	Stim off 2	Stim off 3
High dB	-0.021	-0.014	-0.041	-0.058
Mid dB	-0.079	-0.033	-0.070	-0.016
Low dB	-0.023	-0.023	-0.033	-0.034

Comparison to flat line (p-values)

L2/3	Stim on	Stim off 1	Stim off 2	Stim off 3
High dB	**3.8×10^{-9}**	**1.6×10^{-8}**	**5.7×10^{-4}**	**4.4×10^{-9}**
Mid dB	**3.8×10^{-9}**	**4.5×10^{-6}**	**8.6×10^{-9}**	**6.6×10^{-9}**
Low dB	**1.0×10^{-6}**	**2.3×10^{-3}**	**1.3×10^{-7}**	**3.0×10^{-4}**
L4	Stim on	Stim off 1	Stim off 2	Stim off 3
High dB	5.7×10^{-1}	9.6×10^{-1}	**7.0×10^{-4}**	**6.7×10^{-4}**
Mid dB	**4.3×10^{-5}**	6.9×10^{-1}	**2.4×10^{-8}**	6.9×10^{-1}
Low dB	4.6×10^{-1}	8.6×10^{-1}	**7.7×10^{-3}**	8.3×10^{-2}

Comparison p-values

L2/3	Stim on	Stim off 1	Stim off 2	Stim off 3
High - Mid	8.9×10^{-2}	3.5×10^{-1}	1.9×10^{-2}	9.3×10^{-1}
High - Low	3.7×10^{-2}	1.3×10^{-2}	1.1×10^{-1}	**8.2×10^{-3}**
Mid - Low	**8.5×10^{-5}**	2.6×10^{-1}	7.2×10^{-1}	2.1×10^{-2}

L4	Stim on	Stim off 1	Stim off 2	Stim off 3
High - Mid	**7.8×10^{-3}**	8.5×10^{-1}	3.8×10^{-2}	3.1×10^{-2}
High - Low	9.9×10^{-1}	9.6×10^{-1}	7.8×10^{-1}	3.0×10^{-1}
Mid - Low	1.2×10^{-2}	9.6×10^{-1}	**6.8×10^{-3}**	4.9×10^{-1}

Layer comparison (averaged across dB) slopes

	Stim on	Stim off 1	Stim off 2	Stim off 3
L2/3 slope	-0.077	-0.048	-0.042	-0.077
L4 slope	-0.041	-0.023	-0.048	-0.036
p-val	**8.6×10^{-4}**	1.2×10^{-1}	2.6×10^{-1}	**6.8×10^{-4}**

Comparison to flat line (p-values)

	Stim on	Stim off 1	Stim off 2	Stim off 3
L2/3 p-val	**9.7×10^{-10}**	**1.5×10^{-3}**	**9.6×10^{-10}**	**1.2×10^{-9}**
L4 p-val	**2.4×10^{-5}**	1.8×10^{-1}	**9.6×10^{-10}**	**5.4×10^{-4}**

Supplemental Table 4. Comparison of slopes of MI exclusion plots. All statistical comparisons were done using the analysis of covariance tool in MATLAB (aoctool) and performing a multiple comparisons test with Tukey's honestly significant difference procedure. *Top:* Best fit slopes (bits/%drop out) of the MI exclusion plots at each sound level and statistical comparisons against a line with a zero slope. *Middle:* Statistical comparisons of slopes at each sound level. *Bottom:* Statistical comparisons of slopes between layers from SPL-averaged plots and statistical comparisons against a line with zero slope. Orange background indicates a significant difference at $p<0.01$.

Figures

Figure 1

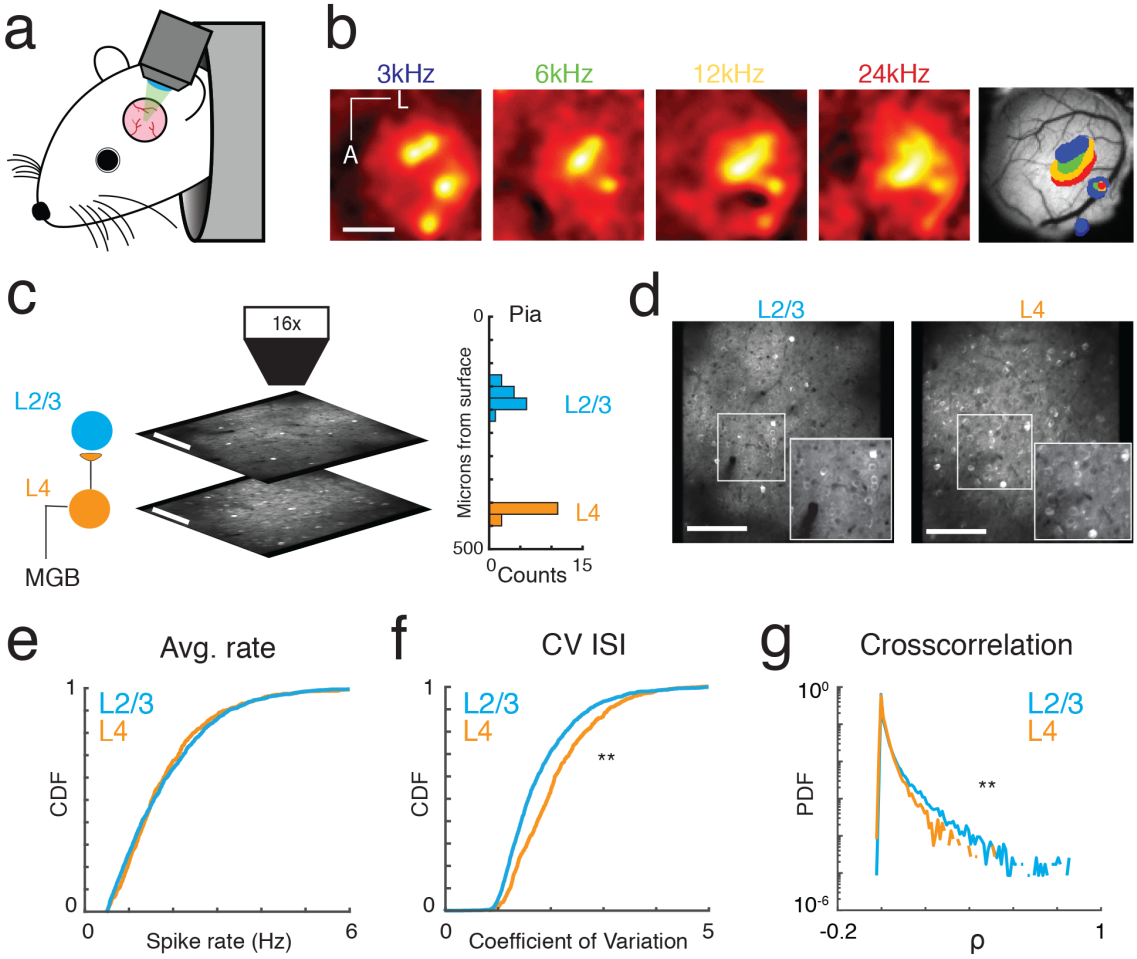

Figure 1. Imaging A1 population activity in the awake mouse. a, Cartoon of awake mouse under the microscope. **b,** Wide-field functional imaging identifies A1. Average activation maps from 4 different sound frequencies and thresholded activity overlaid on image of brain surface. Tonotopic gradient indicates location of A1. Scale bar = 1 mm. **c,** Imaging L4 and L2/3. Histogram shows distribution of imaging plane depths across all experiments. **d,** Representative fields of view from L2/3 (left) and L4 (right) showing GCaMP6s expression present in both layers. Scale bar: 100μm. **e,** Cumulative probability distributions of average λ for all recorded neurons in L2/3 (blue) and L4

(orange) during ongoing activity. **f,** Corresponding cumulative probability distribution of inferred CV inter-spike interval (CV_{ISI}) for all neurons in L4 (orange) and L2/3 (blue). **g,** Probability distribution of pairwise cross-correlation values for all neurons and experiments for L4 (orange) and L2/3 (blue).

Figure 2

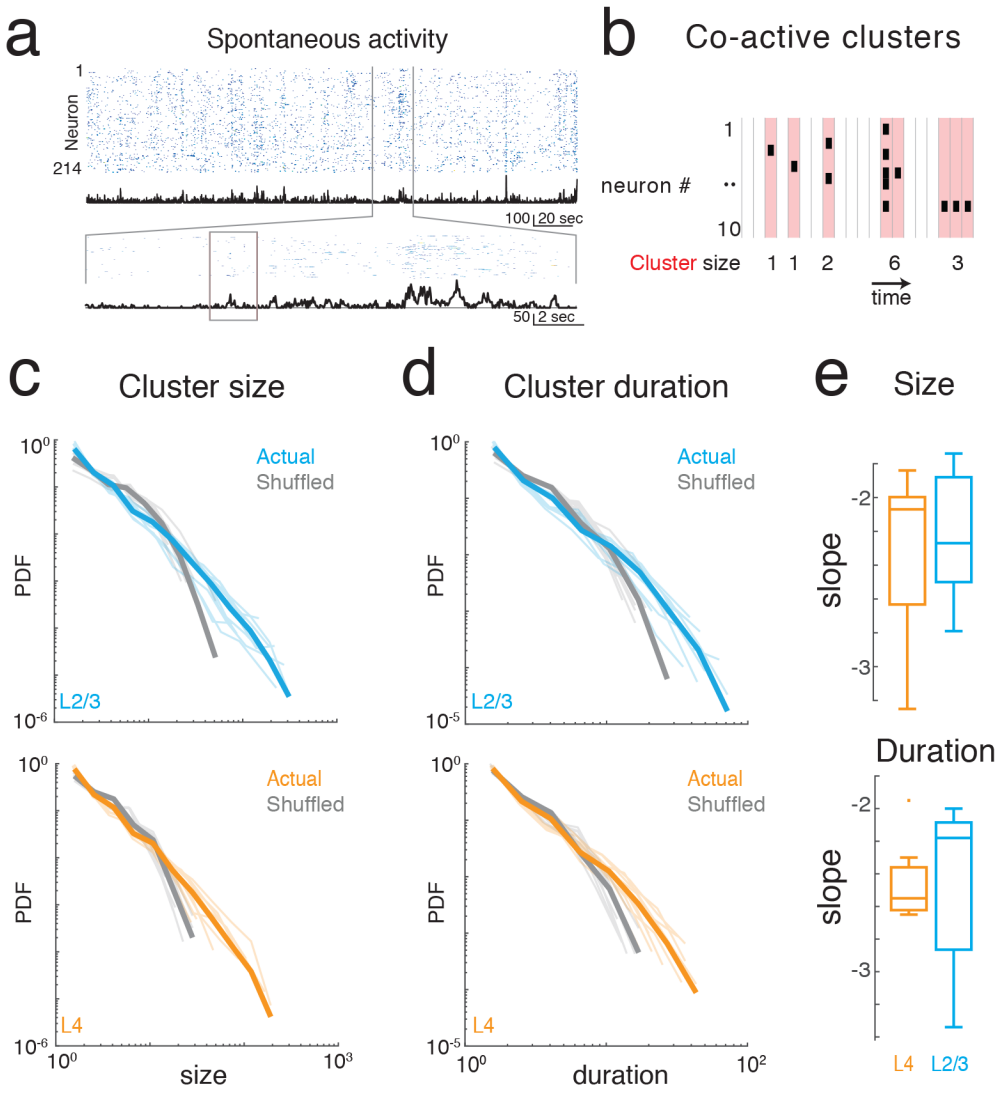

Figure 2. Imaging neuronal ensemble activity in awake mouse A1. a, *Top:* Binarized raster plot of ongoing activity recorded from L2/3 pyramidal neurons with corresponding population activities (black). *Middle:* Expanded view of raster plot revealing variable ongoing activity with population activities. **b,** Schematic depicting definition of activity clusters from a neuronal activity raster. Activity from successive time bins/frames in which at least one neuron is firing (black rectangles) is concatenated into an activity cluster (shading; 5 clusters shown). Clusters are separated by at least 1 frame with no

activity. Vertical gray lines indicate boundaries of frame acquisition (Δt, 33 ms). Cluster sizes defined as the number of spikes in each cluster are indicated below. **c,** Probability density distributions of cluster sizes from individual experiments in L4 and in L2/3. Gray lines indicate distributions from shuffled data. **d**, Probability distributions of activity cluster duration of ongoing activity from all experiments in L2/3 and in L4. Gray lines indicate distributions from shuffled data. Faded lines indicate individual experiments. **e,** Boxplots showing slopes of probability distributions in cluster size (*top*) and cluster duration (*bottom*) for each individual experiment in L4 (orange) and L2/3 (blue), Size: $\alpha_{L2/3}$: –2.23 ± 0.39, α_{L4}: –2.33 ± 0.52, Life: $\alpha_{L2/3}$: –2.47 ± 0.49, α_{L4}: –2.46 ± 0.26, mean±std $p>0.65$, unpaired two-sample t-test.

Figure 3

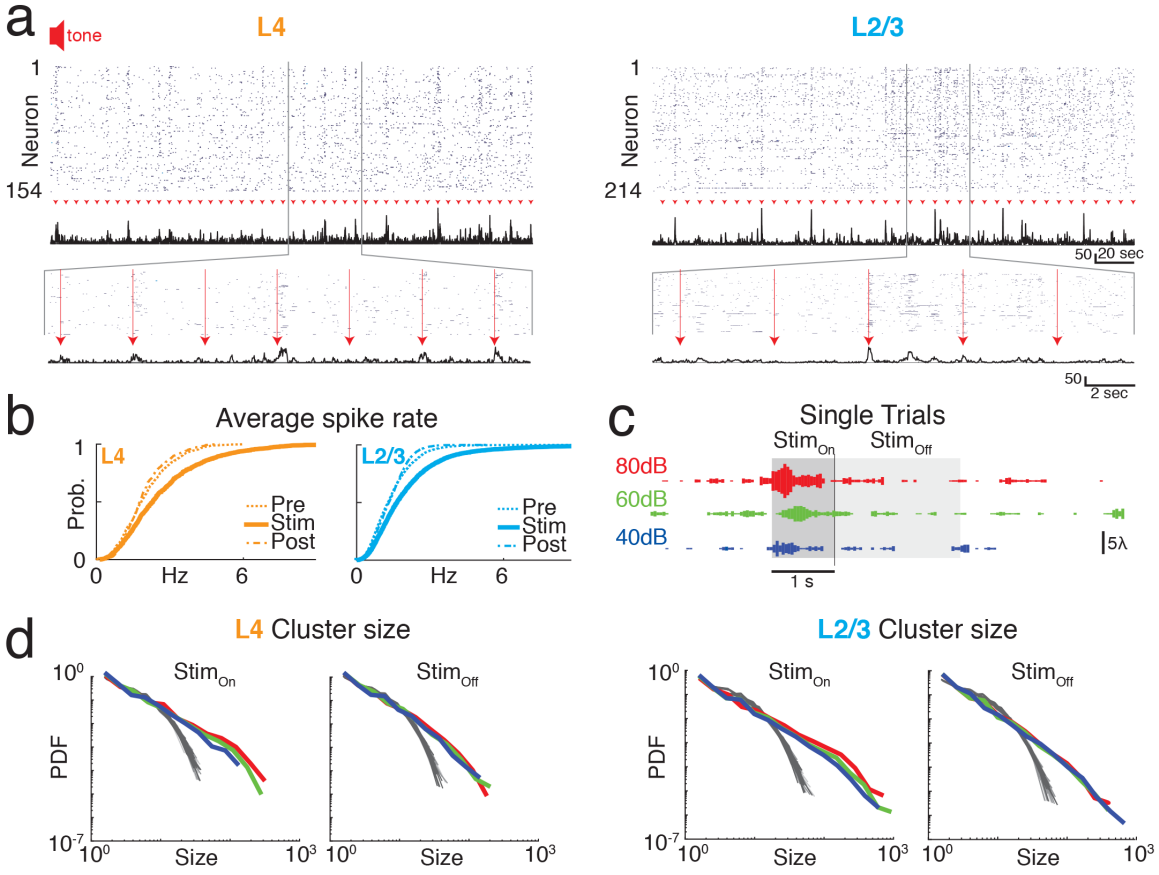

Figure 3. Neuronal ensembles in A1 during ongoing activity organize as neuronal

avalanches. **a,** Binarized raster of simultaneously recorded L4 (*left*) and L2/3 (*right*) neurons to brief auditory inputs (*arrow heads*). *Middle*: Corresponding population activities summed over all neurons. *Bottom*: Enlarged views revealing variable, transient evoked responses. **b,** Stimulation (*Stim*) induces transient rate increases in L4 and L2/3 with post-stimulus rates (*post*) returning to pre-stim baseline (*pre*). Cumulative spike probability plots (all neurons; all stimuli). **c,** Examples of intermittent spiking during stim off at all three sound levels. Single trial time course of the number of active neurons per frame (L2/3) at three different sound levels (color coded). **d,** Probability density distributions of spike cluster sizes reveal power laws for $Stim_{On}$ and $Stim_{Off}$ conditions and different sound intensity in L4 (*left*) and L2/3 (*right*). Gray lines indicate probability density distributions from shuffled data sets. See c for sound level color code.

Figure 4

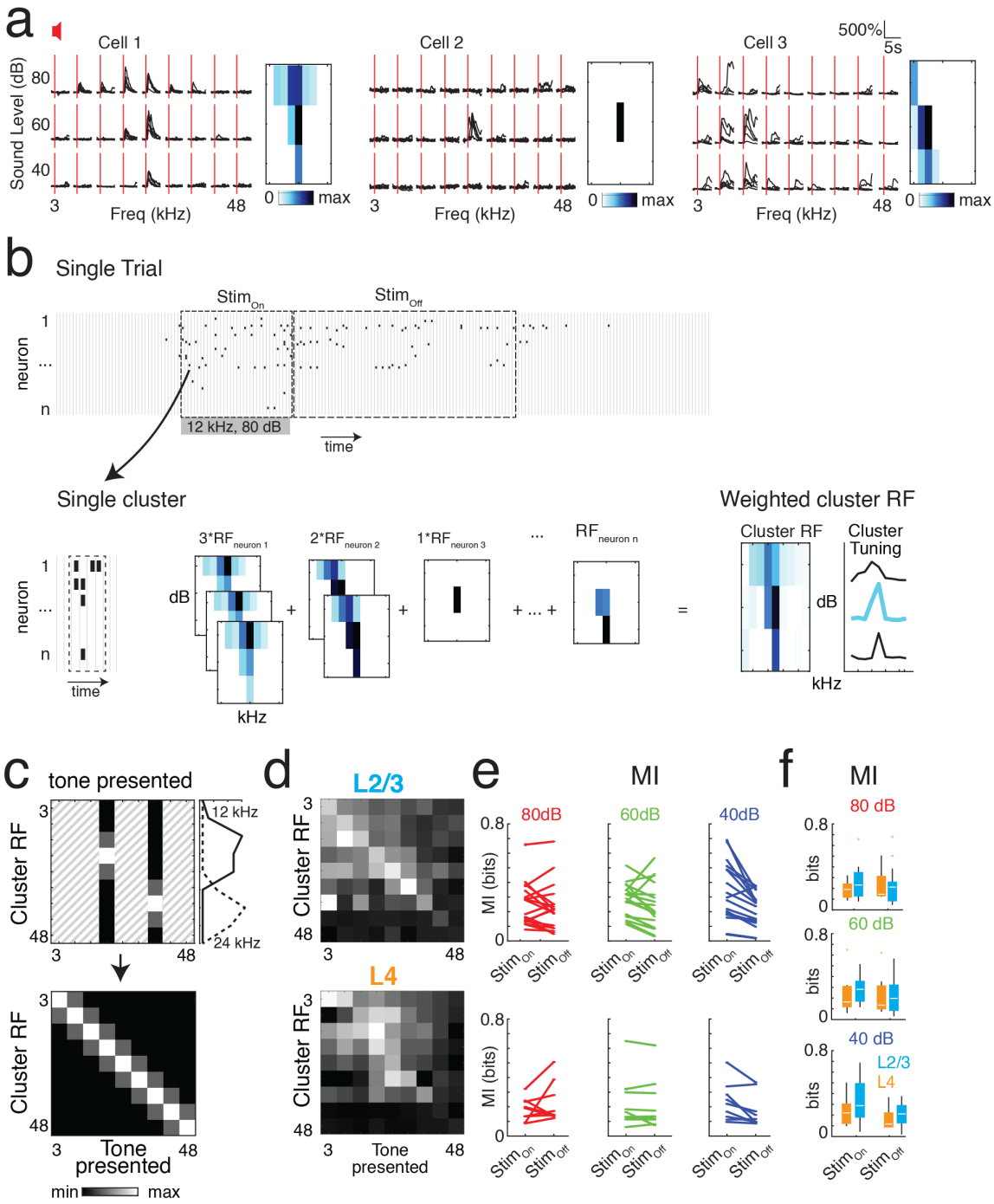

Figure 4. Neuronal avalanches in A1 encode sound information past the stimulus.

a, *Left:* Sound evoked intracellular calcium responses for 3 pyramidal neurons in A1 to 9

different frequencies (column) and 3 sound levels (row). Each black line indicates a single trial; 5 repeats per condition, red line indicates sound stimulus onset. *Right:* Frequency response areas. **b,** Illustration showing the assembly of the cluster RF from the weighted average of the RFs of individual neurons active in the cluster. **c,** Example of assembly of confusion matrix by plotting average Cluster RF as function of presented tone. Top: 12kHz and 24kHz; Bottom: All frequencies. **d,** Example 2-dimensional histograms showing cluster tuning (ordinate) as a function of the stimulus presented (abscissa) in L2/3 and L4 for $Stim_{On}$ period at High sound level (80dB). **e,** Comparisons of MI values derived from confusion matrices during $Stim_{On}$ and $Stim_{Off}$ epochs in individual sessions. Columns represent sound level, rows represent L2/3 (top) or L4 (bottom) (**Supplementary Table 3**). **f,** Comparisons of average MI values during $Stim_{On}$ and $Stim_{Off}$ epochs

Figure 5

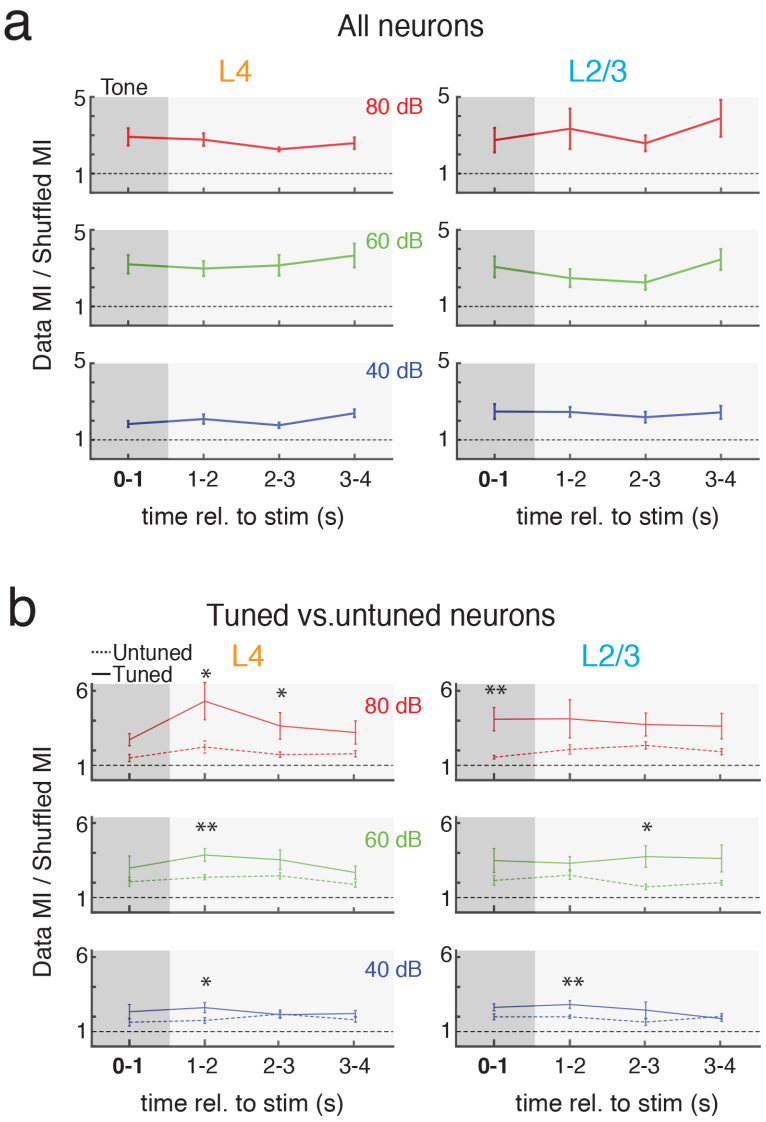

Figure 5. Cluster MI outlasts sound presentation over many seconds. **a,** MI ratio (data MI/shuffled MI) as a function of time for $Stim_{On}$ and $Stim_{Off}$ avalanches in L2/3 and L4 (columns) for different sound levels (rows). Total time after the stimulus turned off ($Stim_{Off}$ period) was divided into 1 s epochs. Dashed line indicates ratio = 1. Error bars indicate STD. Note significant MI ratio above 1 up to 3 s after stimulus off independent of sound level. **b,** Tuned neurons (solid lines) tend to carry more MI compared to

untuned neurons (dashed lines). Conventions as in **a** using only tuned or untuned neurons respectively.

Figure 6

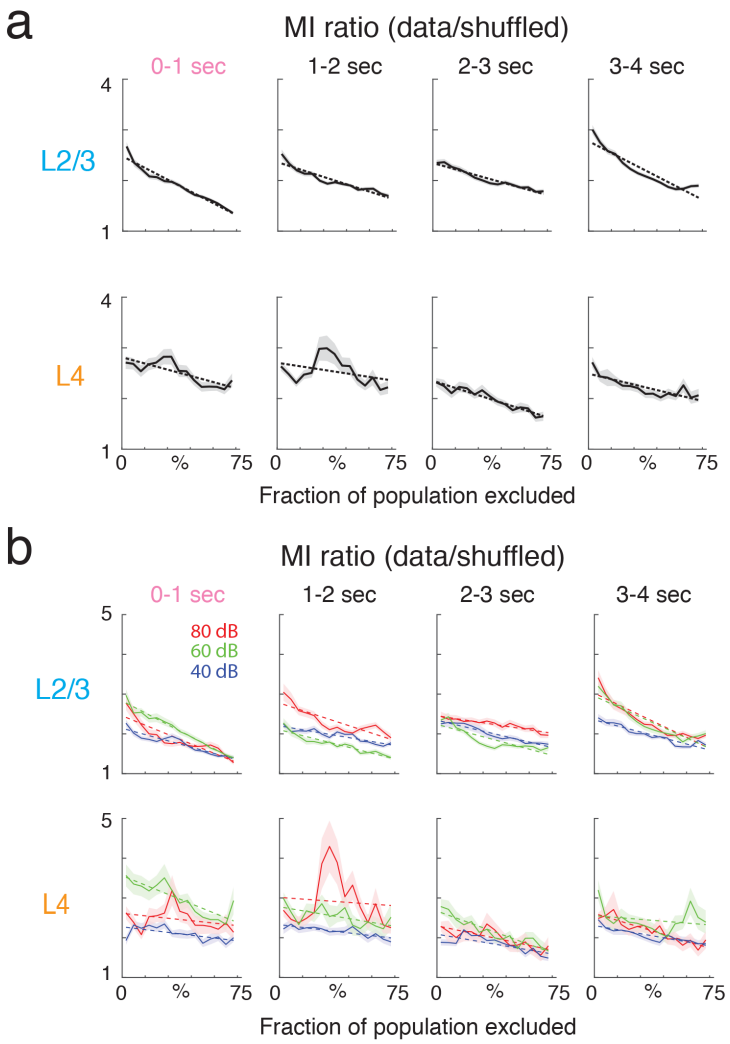

Figure 6. Most active neurons preferentially carry cluster MI in L2/3 and L4. a, Change in MI ratio when removing neurons based on their mean firing rate from the population for different time epochs (columns) for L2/3 (top) and L4 (bottom). Note that even 25% of the least active neurons still carry significant MI. Thick lines: mean across all sound levels. Dashed line: best linear fit (Supplemental Table 4 for sound level comparisons). Neurons were sorted according to their mean λ across the entire imaging session. Most active neurons were removed first. Shading indicates SEM. **b,** MI dependence on neuron activity is independent of sound level. Conventions as in *a* separated by sound level (color coded).

Figure S1

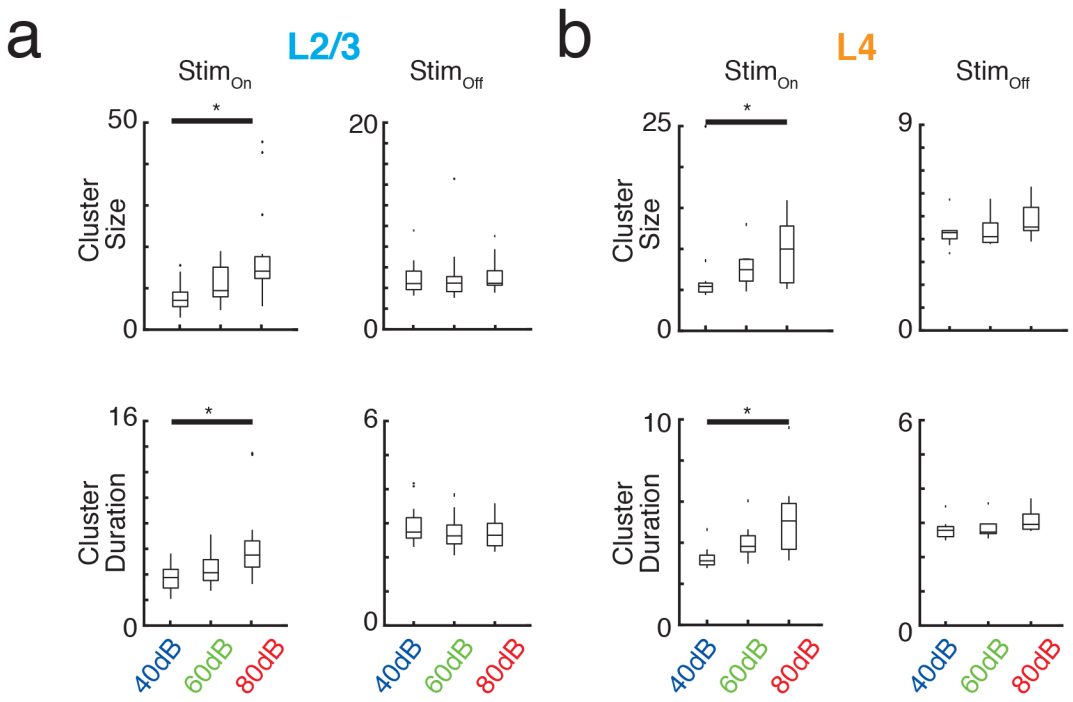

Supplemental Figure 1. Average activity cluster size and duration depend on sound level. **a,** Boxplots showing average cluster size (top row) and average cluster duration (bottom row) in L2/3 neurons as a function of sound level for $Stim_{On}$ (left) and $Stim_{Off}$ (right) periods. **b,** Conventions as in **a**, but for L4 neurons.

References

Aquino G, Bologna M, Grigolini P, West BJ. 2010. Beyond the Death of Linear Response: 1/f Optimal Information Transport. Physical Review Letters 105.
Aquino G, Bologna M, West BJ, Grigolini P. 2011. Transmission of information between complex systems: 1/f resonance. Phys Rev E Stat Nonlin Soft Matter Phys 83:051130.
Arieli A, Sterkin A, Grinvald A, Aertsen A. 1996. Dynamics of ongoing activity: explanation of the large variability in evoked cortical responses. Science 273:1868-1871.
Atencio CA, Schreiner CE. 2009. Laminar diversity of dynamic sound processing in cat primary auditory cortex. Journal of neurophysiology 103:192-205.
Atencio CA, Sharpee TO, Schreiner CE. 2009. Hierarchical computation in the canonical auditory cortical circuit. Proceedings of the National Academy of Sciences 106:21894.
Bandyopadhyay S, Shamma SA, Kanold PO. 2010. Dichotomy of functional organization in the mouse auditory cortex. Nat Neurosci 13:361-368.
Bartho P, Curto C, Luczak A, Marguet SL, Harris KD. 2009. Population coding of tone stimuli in auditory cortex: dynamic rate vector analysis. Eur J Neurosci 30:1767-1778.
Bartlett EL, Wang X. 2005. Long-lasting modulation by stimulus context in primate auditory cortex. J Neurophysiol 94:83-104.
Bathellier B, Ushakova L, Rumpel S. 2012. Discrete neocortical dynamics predict behavioral categorization of sounds. Neuron 76:435-449.
Beggs JM, Plenz D. 2003. Neuronal avalanches in neocortical circuits. J Neurosci 23:11167-11177.
Bellay T, Klaus A, Seshadri S, Plenz D. 2015. Irregular spiking of pyramidal neurons organizes as scale-invariant neuronal avalanches in the awake state. Elife 4:e07224.
Bernstein JG, Oxenham AJ. 2006. The relationship between frequency selectivity and pitch discrimination: sensorineural hearing loss. J Acoust Soc Am 120:3929-3945.
Brosch M, Schreiner CE. 2000. Sequence sensitivity of neurons in cat primary auditory cortex. Cereb Cortex 10:1155-1167.
Chen TW, Wardill TJ, Sun Y, Pulver SR, Renninger SL, Baohan A, Schreiter ER, Kerr RA, Orger MB, Jayaraman V, Looger LL, Svoboda K, Kim DS. 2013. Ultrasensitive fluorescent proteins for imaging neuronal activity. Nature 499:295-300.
Chialvo DR. 2010. Emergent complex neural dynamics. Nat Phys 6:744-750.
Clauset A, Shalizi C, Newman M. 2009. Power-Law Distributions in Empirical Data. siam review, 51 (4), 661-703. In.
Clawson WP, Wright NC, Wessel R, Shew WL. 2017. Adaptation towards scale-free dynamics improves cortical stimulus discrimination at the cost of reduced detection. Plos Comput Biol 13:e1005574.
Deweese MR, Zador AM. 2004. Shared and private variability in the auditory cortex. J Neurophysiol 92:1840-1855.
Francis NA, Winkowski DE, Sheikhattar A, Armengol K, Babadi B, Kanold PO. 2018. Small Networks Encode Decision-Making in Primary Auditory Cortex. Neuron.
Gautam H, Hoang TT, McClanahan K, Grady SK, Shew WL. 2015. Maximizing Sensory Dynamic Range by Tuning the Cortical State to Criticality. Plos Comput Biol 11.

Goldey GJ, Roumis DK, Glickfeld LL, Kerlin AM, Reid RC, Bonin V, Schafer DP, Andermann ML. 2014. Removable cranial windows for long-term imaging in awake mice. Nat Protoc 9:2515-2538.
Guizar-Sicairos M, Thurman ST, Fienup JR. 2008. Efficient subpixel image registration algorithms. Opt Lett 33:156-158.
Guo ZV, Hires SA, Li N, O'Connor DH, Komiyama T, Ophir E, Huber D, Bonardi C, Morandell K, Gutnisky D, Peron S, Xu NL, Cox J, Svoboda K. 2014. Procedures for behavioral experiments in head-fixed mice. PLoS One 9:e88678.
Jesteadt W, Wier CC, Green DM. 1977. Intensity discrimination as a function of frequency and sensation level. J Acoust Soc Am 61:169-177.
Karimipanah Y, Ma Z, Miller JK, Yuste R, Wessel R. 2017. Neocortical activity is stimulus- and scale-invariant. PLoS One 12:e0177396.
Kinouchi O, Copelli M. 2006. Optimal dynamical range of excitable networks at criticality. Nature Physics 2 348-351.
Klampfl S, David SV, Yin P, Shamma SA, Maass W. 2012. A quantitative analysis of information about past and present stimuli encoded by spikes of A1 neurons. J Neurophysiol 108:1366-1380.
Klaus A, Yu S, Plenz D. 2011. Statistical analyses support power law distributions found in neuronal avalanches. PLoS One 6:e19779.
Levina A, Priesemann V. 2017. Subsampling scaling. Nature Communications 8:15140.
Levy RB, Reyes AD. 2012. Spatial profile of excitatory and inhibitory synaptic connectivity in mouse primary auditory cortex. J Neurosci 32:5609-5619.
Luczak A, Bartho P, Harris KD. 2009. Spontaneous events outline the realm of possible sensory responses in neocortical populations. Neuron 62:413-425.
Maor I, Shalev A, Mizrahi A. 2016. Distinct Spatiotemporal Response Properties of Excitatory Versus Inhibitory Neurons in the Mouse Auditory Cortex. Cereb Cortex.
Martin KA, Schroder S. 2013. Functional heterogeneity in neighboring neurons of cat primary visual cortex in response to both artificial and natural stimuli. J Neurosci 33:7325-7344.
Martinello M, Hidalgo J, Maritan A, di Santo S, Plenz D, Muñoz MA. 2017. Neutral Theory and Scale-Free Neural Dynamics. Physical Review X 7:041071.
Meng X, Winkowski DE, Kao JPY, Kanold PO. 2017. Sublaminar Subdivision of Mouse Auditory Cortex Layer 2/3 Based on Functional Translaminar Connections. J Neurosci 37:10200-10214.
Nelken I, Fishbach A, Las L, Ulanovsky N, Farkas D. 2003. Primary auditory cortex of cats: feature detection or something else? Biol Cybern 89:397-406.
Ohki K, Chung S, Ch'ng YH, Kara P, Reid RC. 2005. Functional imaging with cellular resolution reveals precise micro-architecture in visual cortex. Nature 433:597-603.
Oswald AM, Doiron B, Rinzel J, Reyes AD. 2009. Spatial profile and differential recruitment of GABAB modulate oscillatory activity in auditory cortex. J Neurosci 29:10321-10334.
Pachitariu M, Stringer C, Harris KD. 2018. Robustness of Spike Deconvolution for Neuronal Calcium Imaging. The Journal of Neuroscience 38:7976.
Pachitariu M, Stringer, C., Harris, K.D. 2017. Robustness of spike deconvolution for calcium imaging of neural spiking. bioRxiv.

Peron S, Chen T-W, Svoboda K. 2015. Comprehensive imaging of cortical networks. Current opinion in neurobiology 32:115-123.
Petermann T, Thiagarajan T, Lebedev MA, Nicolelis MA, Chialvo DR, Plenz D. 2009. Spontaneous cortical activity in awake monkeys composed of neuronal avalanches. ProcNatlAcadSciUSA 106:15921-15926.
Petrus E, Isaiah A, Jones AP, Li D, Wang H, Lee HK, Kanold PO. 2014. Crossmodal induction of thalamocortical potentiation leads to enhanced information processing in the auditory cortex. Neuron 81:664-673.
Priesemann V, Munk MH, Wibral M. 2009. Subsampling effects in neuronal avalanche distributions recorded in vivo. BMCNeurosci 10:40.
Quian Quiroga R, Panzeri S. 2009. Extracting information from neuronal populations: information theory and decoding approaches. Nat Rev Neurosci 10:173-185.
Ratzlaff EH, Grinvald A. 1991. A tandem-lens epifluorescence macroscope: hundred-fold brightness advantage for wide-field imaging. J Neurosci Methods 36:127-137.
Ribeiro TL, Copelli M, Caixeta F, Belchior H, Chialvo DR, Nicolelis MA, Ribeiro S. 2010. Spike avalanches exhibit universal dynamics across the sleep-wake cycle. PLoS One 5:e14129.
Ribeiro TL, Ribeiro S, Belchior H, Caixeta F, Copelli M. 2014. Undersampled Critical Branching Processes on Small-World and Random Networks Fail to Reproduce the Statistics of Spike Avalanches. PLoS One 9:e94992.
Rose T, Jaepel J, Hubener M, Bonhoeffer T. 2016. Cell-specific restoration of stimulus preference after monocular deprivation in the visual cortex. Science 352:1319-1322.
Rothschild G, Nelken I, Mizrahi A. 2010. Functional organization and population dynamics in the mouse primary auditory cortex. Nat Neurosci 13:353-360.
Schindelin J, Arganda-Carreras I, Frise E, Kaynig V, Longair M, Pietzsch T, Preibisch S, Rueden C, Saalfeld S, Schmid B, Tinevez JY, White DJ, Hartenstein V, Eliceiri K, Tomancak P, Cardona A. 2012. Fiji: an open-source platform for biological-image analysis. Nat Methods 9:676-682.
Schreiber T, Schmitz A. 2000. Surrogate time series. Physica D 142:346-382.
Seshadri S, Klaus A, Winkowski DE, Kanold PO, Plenz D. 2018. Altered avalanche dynamics in a developmental NMDAR hypofunction model of cognitive impairment. Transl Psychiatry 8:3.
Shew WL, Bellay T, Plenz D. 2010. Simultaneous multi-electrode array recording and two-photon calcium imaging of neural activity. J Neurosci Methods 192:75-82.
Shew WL, Clawson WP, Pobst J, Karimipanah Y, Wright NC, Wessel R. 2015. Adaptation to sensory input tunes visual cortex to criticality. Nat Phys:doi:10.1038/nphys3370.
Shew WL, Plenz D. 2013. The functional benefits of criticality in the cortex. Neuroscientist 19:88-100.
Shew WL, Yang H, Petermann T, Roy R, Plenz D. 2009. Neuronal avalanches imply maximum dynamic range in cortical networks at criticality. J Neurosci 29:15595-15600.
Shew WL, Yang H, Yu S, Roy R, Plenz D. 2011. Information capacity and transmission are maximized in balanced cortical networks with neuronal avalanches. J Neurosci 31:55-63.

Shriki O, Alstott J, Carver F, Holroyd T, Henson RN, Smith ML, Coppola R, Bullmore E, Plenz D. 2013. Neuronal avalanches in the resting MEG of the human brain. J Neurosci 33:7079-7090.
Shriki O, Yellin D. 2016. Optimal Information Representation and Criticality in an Adaptive Sensory Recurrent Neuronal Network. Plos Comput Biol 12:e1004698.
Suter BA, O'Connor T, Iyer V, Petreanu LT, Hooks BM, Kiritani T, Svoboda K, Shepherd GM. 2010. Ephus: multipurpose data acquisition software for neuroscience experiments. Front Neural Circuits 4:100.
Thevenaz P, Ruttimann UE, Unser M. 1998. A pyramid approach to subpixel registration based on intensity. IEEE Trans Image Process 7:27-41.
Touboul J, Destexhe A. 2010. Can power-law scaling and neuronal avalanches arise from stochastic dynamics? PLoS ONE 5:e8982.
Touboul J, Destexhe A. 2017. Power-law statistics and universal scaling in the absence of criticality. Phys Rev E 95.
Vogelstein JT, Packer AM, Machado TA, Sippy T, Babadi B, Yuste R, Paninski L. 2010. Fast nonnegative deconvolution for spike train inference from population calcium imaging. J Neurophysiol 104:3691-3704.
Wang X. 2007. Neural coding strategies in auditory cortex. Hear Res 229:81-93.
Wang X, Lu T, Snider RK, Liang L. 2005. Sustained firing in auditory cortex evoked by preferred stimuli. Nature 435:341-346.
Watkins PV, Kao JP, Kanold PO. 2014. Spatial pattern of intra-laminar connectivity in supragranular mouse auditory cortex. Front Neural Circuits 8:15.
West BJ, Geneston EL, Grigolini P. 2008. Maximizing information exchange between complex networks. Physics Reports 468:1-99.
Wier CC, Jesteadt W, Green DM. 1977. Frequency discrimination as a function of frequency and sensation level. J Acoust Soc Am 61:178-184.
Winkowski DE, Kanold PO. 2013. Laminar transformation of frequency organization in auditory cortex. J Neurosci 33:1498-1508.
Yu S, Ribeiro TL, Meisel C, Chou S, Mitz A, Saunders R, Plenz D. 2017. Maintained avalanche dynamics during task-induced changes of neuronal activity in nonhuman primates. eLife 6:e27119.
Zylberberg J. 2017. Untuned But Not Irrelevant: The Role of Untuned Neurons In Sensory Information Coding. bioRxiv.